



Review

# Recent Developments in Lanthanide-Doped Alkaline Earth Aluminate Phosphors with Enhanced and Long-Persistent Luminescence

Doory Kim <sup>1,2,3,4</sup><sup>1</sup> Department of Chemistry, Hanyang University, Seoul 04763, Korea; doorykim@hanyang.ac.kr<sup>2</sup> Research Institute for Convergence of Basic Sciences, Hanyang University, Seoul 04763, Korea<sup>3</sup> Institute of Nano Science and Technology, Hanyang University, Seoul 04763, Korea<sup>4</sup> Research Institute for Natural Sciences, Hanyang University, Seoul 04763, Korea

**Abstract:** Lanthanide-activated alkaline earth aluminate phosphors are excellent luminescent materials that are designed to overcome the limitations of conventional sulfide-based phosphors. The increasing research attention on these phosphors over the past decade has led to a drastic improvement in their phosphorescence efficiencies and resulted in a wide variety of phosphorescence colors, which can facilitate applications in various areas. This review article discusses the development of lanthanide-activated alkaline earth aluminate phosphors with a focus on the various synthesis methods, persistent luminescence mechanisms, activator and coactivator effects, and the effects of compositions. Particular attention has been devoted to alkaline earth aluminate phosphors that are extensively used, such as strontium-, calcium-, and barium-based aluminates. The role of lanthanide ions as activators and coactivators in phosphorescence emissions was also emphasized. Finally, we address recent techniques involving nanomaterial engineering that have also produced lanthanide-activated alkaline earth aluminate phosphors with long-persistent luminescence.

**Keywords:** lanthanide doping; strontium aluminates; calcium aluminates; barium aluminates; synthesis; phosphors; long-persistent luminescence; phosphorescence



**Citation:** Kim, D. Recent Developments in Lanthanide-Doped Alkaline Earth Aluminate Phosphors with Enhanced and Long-Persistent Luminescence. *Nanomaterials* **2021**, *11*, 723. <https://doi.org/10.3390/nano11030723>

Academic Editor: Tomasz Grzyb

Received: 8 February 2021

Accepted: 9 March 2021

Published: 13 March 2021

**Publisher's Note:** MDPI stays neutral with regard to jurisdictional claims in published maps and institutional affiliations.



**Copyright:** © 2021 by the author. Licensee MDPI, Basel, Switzerland. This article is an open access article distributed under the terms and conditions of the Creative Commons Attribution (CC BY) license (<https://creativecommons.org/licenses/by/4.0/>).

## 1. Introduction

Phosphorescence involves the emission of light for significant periods of time, even after removal of the exciting radiation. Unlike fluorophores, phosphors can store the absorbed light energy and release it as long-persistent luminescence in the form of a delayed weak radiation via forbidden energy state transitions. Such persistent, luminescent, and phosphorescent materials with an adequate lifetime have attracted considerable attention for a wide range of applications, such as devices based on organic light-emitting diodes (OLEDs) and in solar cells for energy conservation and emergency lighting.

Natural phosphorescence was first observed by Cellini in diamond in 1568, and several natural minerals have also been reported to generate similar emissions of light under illumination with sunlight, such as naturally doped willemite, scheelite, and calcite crystals [1]. The first artificial phosphor was synthesized via calcination of sulfur-rich barium sulfate in 1604 [2]. Sulfide-based phosphors, such as rare-earth alkali sulfides (CaS, SrS) and zinc sulfides doped with copper and cobalt (ZnS:Cu, ZnS:Co), were subsequently synthesized in the first half of the 20th century [3]. Among these, copper-doped zinc sulfide (ZnS:Cu) phosphors have been extensively employed as long-lasting phosphorescent materials in various areas, such as flat panel displays, cathode ray tubes, fluorescent lamps, and traffic signs [4]. Its afterglow intensity is known to be enhanced by doping with transition metals (such as cobalt) and radioactive elements (such as promethium); however, the mechanical and physical properties of the host are degraded when a large amount of a dopant is incorporated, which eventually leads to the rapid degradation of its chemical

stability [5]. In addition, the low emission intensity and short intrinsic time of decay (1 h) of ZnS:Cu limit its applications [5].

Rare-earth-doped alkaline earth aluminates have been developed as potential phosphors to overcome such limitations. When alkaline earth aluminates ( $MA_2O_4$ ) are doped with rare-earth ions, the resulting structures can exhibit persistent luminescence for significantly long durations under sunlight illumination, thereby leading to them being considered as excellent luminescent materials [6–10]. Rare-earth elements are a group of 17 elements consisting of lanthanides, yttrium (Y), and scandium (Sc). Europium-doped strontium aluminates ( $SrAl_2O_4:Eu^{2+}$ ) were synthesized and studied as the first rare-earth-doped strontium aluminates in the late 1960s [11]. This development can be considered a breakthrough in the field of phosphorescence in terms of the applications of phosphor, primarily because of the high luminescence efficiency of such phosphors, which was ~10 times that of zinc sulfide; such phosphors also exhibited high chemical and physical stability [12]. Moreover, these phosphors are environmentally friendly, thanks to their low chemical toxicities and the lack of radioactive elements [13]. Particularly, the development of codoped  $SrAl_2O_4:Eu^{2+},Dy^{3+}$  (Dy: dysprosium) phosphors by Matsuzawa et al. has received considerable attention for the replacement of traditional ZnS-based phosphors, owing to their improved afterglow intensities, lifetimes, and chemical stabilities compared to those of the previously synthesized phosphors [5]. The intense emission of rare-earth-based phosphor has led to extensive applications in light-emitting diode (LED) devices, thin-film electroluminescent (TFEL) devices, optoelectronic or cathodoluminescent devices, safety marks, radiation dosimetry, X-ray imaging, bioimaging, and photodynamic therapy [14–19]. In particular, their applications as LED devices can help in replacing argon-mercury discharge fluorescent lamps, which are extensively used for general lighting purposes. They can also be applied as alternative mercury-free excitation sources for avoiding the use of hazardous ingredients and environmentally unsafe materials [20]. Moreover, they have been recently demonstrated as solar cell materials and high upconversion luminescent materials [21,22].

The phosphorescence from such lanthanide-activated alkaline earth aluminate phosphors can be tuned over the emission wavelength and lifetime, based on the 4f–5d transitions of lanthanides. The 4f–5d optical transition is electric-dipole allowed and, therefore, generally features a high radiative emission probability and short lifetime (of the order of tens of nanoseconds) [23–25]. This transition generates significantly broader absorption and emission spectra because of the high sensitivity of the 5d orbital to the surrounding environment. The luminescence properties arising from the 4f–5d transition of lanthanides can be tuned by varying the host material and lanthanide emitters. In particular, the luminescence properties arising from the 4f–5d transition of  $Eu^{2+}$  have been investigated in more than 300 compounds, and various emission colors from near-ultraviolet to deep red have been revealed [26].

Therefore, in this review, lanthanide-doped alkaline earth aluminate phosphors are discussed in the context of their potential as excellent luminescent materials. Lanthanide-doped strontium aluminate-, calcium aluminate-, and barium-aluminate-based phosphors are focused on, and their synthesis techniques, phosphorescence mechanisms, and effects of dopants and codopants are reviewed. Recent advances in the synthesis of lanthanide-doped alkaline earth aluminate phosphors are also highlighted. Finally, we discuss the prospects and challenges of the future development of lanthanide-doped alkaline earth aluminate phosphors.

## 2. Strontium Aluminate Phosphors

Strontium aluminates are the most extensively used alkaline earth aluminates and are convenient host crystals for rare-earth dopants [27]. They have attracted recent research interest that has resulted in their extensive applications in several fields owing to their excellent phosphor properties such as high brightness, long-persistent luminescence, and good chemical stability compared to those of other phosphor materials (Table 1). There are various types of strontium aluminate hosts, such as  $SrAl_2O_4$ ,  $SrAl_2B_2O_7$ ,  $SrAl_4O_7$ ,  $SrAl_{12}O_{19}$ ,

$\text{Sr}_3\text{Al}_2\text{O}_6$ , and  $\text{Sr}_4\text{Al}_{14}\text{O}_{25}$ , all of which have different structures. For example,  $\text{SrAl}_2\text{O}_4$  has a tridymite structure, whereas  $\text{SrAl}_{12}\text{O}_{19}$  has a magnetoplumbite structure [28,29]. Among these,  $\text{SrAl}_2\text{O}_4$  is a promising host material for ensuring persistent luminescence and acts as a convenient host crystal for rare-earth and transition metal dopants [30].

**Table 1.** Comparison of reported studies for the synthesis of lanthanide-doped strontium aluminate phosphors.

Host Material	Activator	Co-Activator	Synthesis Method	Color or $\lambda$	Remarks	Ref
SrAl <sub>2</sub> O <sub>4</sub>	Eu <sup>2+</sup>	-	Solid-state reaction (1300 °C)	Green ( $\lambda_{em} = 515$ nm(295 K) $\lambda_{em} = 445$ nm(20 K))	It was found that the luminescent center is the same, but excitation processes are different at different temperatures.	[31]
			Solid-state reaction (1250 °C)	Green ( $\lambda_{em} = 512$ nm)	The position of the Eu 4f states showed the charge transfer transition.	[28]
			Combustion method (600 °C)	Green ( $\lambda_{ex} = 360$ nm, $\lambda_{em} = 513$ nm)	The ratio of Eu <sup>2+</sup> to Eu <sup>3+</sup> is changed depending on the total concentration of Eu dopants, determining the luminescence color of the phosphors.	[32]
			Combustion method using urea at 500 °C and calcinated at 1000 °C	Green ( $\lambda_{em} = 520$ nm)	The luminescence mechanism and temperature dependence of bands intensities are discussed on the crystal field theory and the vibronic approach.	[7]
	Dy <sup>3+</sup>	-	Combustion method (600 °C)	$\lambda_{ex} = 356$ nm, $\lambda_{em} = 480$ nm, 573 nm, 670 nm	The piezo-electricity was suggested to be responsible for producing mechanoluminescence in prepared phosphor.	[27]
	Tb <sup>3+</sup>	-	Precursor route via the thermal decomposition of tartarate compounds	$\lambda_{em} = 542$ nm	They demonstrated that the precursor method via the thermal decomposition of multimetallic tartarate compounds is a quick, simple and inexpensive way for the preparation of alkaline-earth aluminate powder.	[33]
	Eu <sup>2+</sup> or Ce <sup>3+</sup>	-	Combustion method (600 °C)	Eu <sup>2+</sup> : $\lambda_{ex} = 230$ , 350 nm, $\lambda_{em} = 498$ nm, Ce <sup>3+</sup> : $\lambda_{ex} = 266$ , 331 nm, $\lambda_{em} = 371$ nm	Experimental results matched with the predictions of Dorenbos' model.	[30]
	Eu <sup>2+</sup> or Nd <sup>3+</sup>	-	Solid-state reaction (1000 °C)	-	The structures of the alkaline earth aluminates were systematically studied using a combination of synchrotron X-ray and neutron powder diffraction.	[13]

Table 1. Cont.

Host Material	Activator	Co-Activator	Synthesis Method	Color or $\lambda$	Remarks	Ref
SrAl <sub>2</sub> O <sub>4</sub>	Eu <sup>2+</sup>	Dy <sup>3+</sup>	Solid-state reaction (1300 °C)	Green ( $\lambda_{\text{ex}} = 365 \text{ nm}$ , $\lambda_{\text{em}} = 520 \text{ nm}$ )	They observed that Dy <sup>3+</sup> ion creates the highly dense trapping level by acting as the hole-trap.	[5]
			Floating zone technique	Green ( $\lambda_{\text{em}} = 520 \text{ nm}$ )	The intensities and the persistent times of the phosphorescences are found to depend on the growth atmosphere.	[34]
			Laser-heated pedestal growth method	Green ( $\lambda_{\text{em}} = 520 \text{ nm}$ )	It was found that multiple trapping centers are involved in the phosphorescence dynamic processes, which are responsible for the long persistence.	[35]
			Solid-state reaction (900–1350 °C)	$\lambda_{\text{em}} = 518 \text{ nm}$	The depth of Dy <sup>3+</sup> trap levels is in the order of BaAl <sub>2</sub> O <sub>4</sub> host > CaAl <sub>2</sub> O <sub>4</sub> host > SrAl <sub>2</sub> O <sub>4</sub> host.	[36]
			Sol-gel method (900–1250 °C)	Green-blue ( $\lambda_{\text{em}} = 511 \text{ nm}$ )	It was found that the single-phase SrAl <sub>2</sub> O <sub>4</sub> was formed at 900 °C, which is 300 °C lower than the required temperature for the conventional solid-state reaction.	[37]
			Combustion method (600 °C)	Yellow-green ( $\lambda_{\text{em}} = 516 \text{ nm}$ )	They proposed that phosphor samples obtain a persistent luminescence with the aid of the energy transfer at the trap level.	[38]
			Combustion method (500 °C)	$\lambda_{\text{em}} = 528 \text{ nm}$	They found that the monoclinic crystal structures of both CaAl <sub>2</sub> O <sub>4</sub> and SrAl <sub>2</sub> O <sub>4</sub> are more appropriate in creating the traps, which is directly related to the long afterglow phenomena.	[39]
			Laser synthesis	Green ( $\lambda_{\text{em}} = 520 \text{ nm}$ )	This laser melting method is a promising route for the synthesis of ceramic phosphors.	[40]
			Solid-state reaction (~1300 °C)	Green ( $\lambda_{\text{em}} = 520 \text{ nm}$ )	A systematic investigation of the composition of phosphors, such as the concentrations of Eu <sup>2+</sup> , Dy <sup>3+</sup> , alkali metal, alkaline earth metal, Si ions.	[12]
			Flame spray pyrolysis technique	Green ( $\lambda_{\text{em}} = 525 \text{ nm}$ )	The flame spray pyrolysis technique was demonstrated to manufacture the rounded and spherical particles of SrAl <sub>2</sub> O <sub>4</sub> :Eu <sup>2+</sup> /Dy <sup>3+</sup> phosphor without any problem.	[41]

Table 1. Cont.

Host Material	Activator	Co-Activator	Synthesis Method	Color or $\lambda$	Remarks	Ref
SrAl <sub>2</sub> O <sub>4</sub>	Eu <sup>2+</sup>	Nd <sup>3+</sup>	Combustion method (550 °C)	Green-blue ( $\lambda_{\text{ex}} = 280$ nm, $\lambda_{\text{em}} = 612$ nm)	Nd <sup>3+</sup> trap levels can be thought of as the lanthanide element that causes long phosphorescence at room temperature.	[42]
		Na <sup>+</sup>	Solid-state reaction followed by ball-milling	Green ( $\lambda_{\text{em}} = 520$ nm)	This report presents the factors affecting the luminescence properties of the Eu <sup>2+</sup> -, R <sup>3+</sup> -doped SrAl <sub>2</sub> O <sub>4</sub> .	[43]
		Dy <sup>3+</sup> or Nd <sup>3+</sup>	Combustion method followed by annealing at 1150 °C	Green (Dy <sup>3+</sup> : $\lambda_{\text{em}} = 515$ nm, Nd <sup>3+</sup> : $\lambda_{\text{em}} = 480$ nm)	Eu <sup>2+</sup> photoluminescence is observed to be shifted in a monoclinic/orthorhombic structure.	[44]
		Dy <sup>3+</sup> , Tb <sup>3+</sup>	Combustion method (600 °C)	Green ( $\lambda_{\text{em}} = 513$ nm)	Compared with SrAl <sub>2</sub> O <sub>4</sub> :Eu <sup>2+</sup> , Dy <sup>3+</sup> phosphor, the initial luminescence brightness improved, and the long afterglow time was prolonged in SrAl <sub>2</sub> O <sub>4</sub> :Eu <sup>2+</sup> , Tb <sup>3+</sup> phosphor.	[45]
		La <sup>3+</sup> -Lu <sup>3+</sup> , Y <sup>3+</sup> ; excluding Pm <sup>3+</sup> and Eu <sup>3+</sup>	Solid-state reaction (1250–1300 °C)	Green ( $\lambda_{\text{em}} = 520$ nm)	The co-doping by Dy <sup>3+</sup> intensifies the luminescence by an order of magnitude, whereas the easily reducible rare earths, such as Sm <sup>3+</sup> and Yb <sup>3+</sup> , suppressed both the afterglow and the thermoluminescence.	[46]
Sr <sub>4</sub> Al <sub>14</sub> O <sub>25</sub>	Eu <sup>2+</sup>	Dy <sup>3+</sup> , Er <sup>3+</sup>	Solid-state reaction (1300 °C)	Green-blue ( $\lambda_{\text{em}} = 481, 492$ nm, and 529 nm)	Appropriate Er <sup>3+</sup> doping significantly enhanced the afterglow performance of the phosphors, but excessive Er <sup>3+</sup> doping caused concentration quenching.	[47]
Sr <sub>4</sub> Al <sub>2</sub> O <sub>7</sub>	Eu <sup>3+</sup> , Eu <sup>2+</sup>	-	Solid-state reaction (1500 °C)	Red ( $\lambda_{\text{ex}} = 450$ nm, $\lambda_{\text{em}} = 607$ nm)	Sr <sub>4</sub> Al <sub>2</sub> O <sub>7</sub> has higher emission intensity than Sr <sub>3</sub> Al <sub>2</sub> O <sub>6</sub> due to the higher optimum doping concentration of Sr <sub>4</sub> Al <sub>2</sub> O <sub>7</sub> phosphor.	[31]
	Eu <sup>2+</sup>	Ca <sup>2+</sup>	Halide-assisted solid-state reaction (1450 °C)	Red ( $\lambda_{\text{em}} = 610$ nm)	Partial substitution of Sr <sup>2+</sup> by Ca <sup>2+</sup> in Sr <sub>4</sub> Al <sub>2</sub> O <sub>7</sub> :Eu phosphors is found to be an efficient way to increase the proportion of longer wavelength emission and luminescence intensity.	[48]
SrAl <sub>12</sub> O <sub>19</sub>	Eu <sup>2+</sup>	-	Combustion method (500 °C)	Red ( $\lambda_{\text{ex}} = 341$ nm, $\lambda_{\text{em}} = 397$ nm)	Europium ions were found to be present both in divalent as well as trivalent oxidation states in the sample, and Eu <sup>2+</sup> was observed as the dominant luminescent site.	[49]

Table 1. Cont.

Host Material	Activator	Co-Activator	Synthesis Method	Color or $\lambda$	Remarks	Ref
SrAl <sub>2</sub> O <sub>4</sub> , Sr <sub>4</sub> Al <sub>14</sub> O <sub>25</sub>	Eu <sup>2+</sup>	Dy <sup>3+</sup>	Solid-state reaction followed by ball-milling	Green (SrAl <sub>2</sub> O <sub>4</sub> ), Blue (Sr <sub>4</sub> Al <sub>14</sub> O <sub>25</sub> )	The significant loss of luminescence was observed below 2 $\mu$ m average crystallite size, and performance could be partially restored by reductive annealing above 1000 °C.	[50]
Sr <sub>3</sub> Al <sub>2</sub> O <sub>6</sub> , SrAl <sub>2</sub> O <sub>4</sub> , Sr <sub>4</sub> Al <sub>14</sub> O <sub>25</sub>	Eu <sup>2+</sup>	-	Solid-state reaction (1350 °C)	Sr <sub>3</sub> Al <sub>2</sub> O <sub>6</sub> :Eu <sup>2+</sup> : $\lambda_{em}$ = 510 nm Sr <sub>4</sub> Al <sub>14</sub> O <sub>25</sub> :Eu <sup>2+</sup> : $\lambda_{em}$ = 483 nm	The influences of Al/Sr ratio, sintering temperature, the doping concentration of europium ions on structural transformation and luminescent properties of the phosphors were studied.	[51]
SrAl <sub>2</sub> O <sub>4</sub> , Sr <sub>4</sub> Al <sub>4</sub> O <sub>10</sub> , Sr <sub>3</sub> Al <sub>2</sub> O <sub>6</sub>	Ce <sup>3+</sup>	-	Sol-gel synthesis (700–1200 °C)	SrAl <sub>2</sub> O <sub>4</sub> :Ce: $\lambda_{ex}$ = 575~700 nm Sr <sub>3</sub> Al <sub>2</sub> O <sub>6</sub> :Ce: $\lambda_{ex}$ = 585~675 nm Sr <sub>4</sub> Al <sub>4</sub> O <sub>10</sub> :Ce: $\lambda_{ex}$ = 615 nm	The optical reflectance spectra clearly showed the influence of the strontium aluminate matrix on the optical properties of the synthesized phosphors.	[52]
SrAl <sub>2</sub> O <sub>4</sub> , SrAl <sub>4</sub> O <sub>7</sub> , SrAl <sub>12</sub> O <sub>19</sub> , Sr <sub>4</sub> Al <sub>14</sub> O <sub>25</sub>	Eu <sup>2+</sup>	-	Solid-state reaction (SrAl <sub>12</sub> O <sub>19</sub> :1300 °C, Sr <sub>4</sub> Al <sub>14</sub> O <sub>25</sub> :1400 °C, SrAl <sub>2</sub> O <sub>4</sub> :1350 °C) Citric acid method (SrAl <sub>4</sub> O <sub>7</sub> : 1050 °C)	SrAl <sub>12</sub> O <sub>19</sub> : $\lambda_{em}$ = 397 nm SrAl <sub>4</sub> O <sub>7</sub> : $\lambda_{em}$ = 470 nm Sr <sub>4</sub> Al <sub>14</sub> O <sub>25</sub> : $\lambda_{em}$ = 490 nm	The Eu <sup>2+</sup> emission spectra in the other aluminates showed the trend that the Eu <sup>2+</sup> emission shifts to longer wavelengths with an increasing Sr/Al ratio.	[53]

### 2.1. Lanthanide Ion-Doped Strontium Aluminate Phosphors

Eu<sup>2+</sup> has been frequently used as an activator dopant in SrAl<sub>2</sub>O<sub>4</sub> because it exhibits anomalously long phosphorescence. Because the Sr<sup>2+</sup> and Eu<sup>2+</sup> ions have similar ionic radii (1.21 and 1.20 Å, respectively), Eu<sup>2+</sup> ions are very likely to be located in the Sr<sup>2+</sup> positions; this was also confirmed by electron paramagnetic resonance (EPR) measurements [40,54]. Therefore, when Eu<sup>3+</sup> ions are incorporated in the Sr<sup>2+</sup> sites of SrAl<sub>2</sub>O<sub>4</sub>, they are observed to be easily reduced to Eu<sup>2+</sup> [54,55]. In fact, two different sites are available for Sr ions to occupy, and they are slightly different with respect to the individual Sr–O distances (Sr<sup>+</sup> and Sr<sup>2+</sup> sites are coordinated at 6 and 7, respectively) [53]. The incorporation of Eu<sup>2+</sup> ions in these different sites leads to a variation in the luminescent properties from both sites because of their different symmetries and orientations. The incorporated dopant ions are thought to introduce localized states of the bandgap in the host matrix, which facilitate the luminescent properties that arise from the various dopant-incorporated sites in the SrAl<sub>2</sub>O<sub>4</sub> host material [56]. The doping sites in the host material are known to be determined by the host lattice components and the ionic radii of the dopants. For example, Eu<sup>2+</sup>, Eu<sup>3+</sup>, and Dy<sup>3+</sup> are likely to be incorporated in the Sr<sup>2+</sup> sites in the SrAl<sub>2</sub>O<sub>4</sub> matrix because of their similar ionic radii<sup>+</sup> (Eu<sup>2+</sup>: 1.2Å, Eu<sup>3+</sup>: 0.95 Å, Dy<sup>3+</sup>: 0.91 Å, Sr<sup>2+</sup>: 1.18 Å); the dissimilar ionic radii of Al<sup>3+</sup> and O<sup>2-</sup>, compared to those of the dopants, ensure that the incorporation does not occur in their sites (Al<sup>3+</sup>: 0.53 Å, O<sup>2-</sup>: 1.4 Å). This was confirmed by EPR measurements [56].

When the SrAl<sub>2</sub>O<sub>4</sub> host material is doped with Eu<sup>2+</sup>, the Eu<sup>2+</sup> ion plays the role of a luminescence center via its luminescent 4f<sup>6</sup>5d<sup>1</sup> → 4f<sup>7</sup> transition. Therefore, the 5d–4f transitions of Eu<sup>2+</sup> in aluminate and silicate host materials generate similar broad emission

spectra with a maximum in the blue-green region; the emission band is absent in systems without  $\text{Eu}^{2+}$  doping [57]. Moreover, the maximum peak positions are known to vary with the type of host material and are likely dependent on their surrounding configurations, such as symmetry, bond length, coordination, covalence, site size, and crystal field strength [57]. This probably occurs because of the displacement of the 5d energy level of  $\text{Eu}^{2+}$  in different crystal fields [56]. Therefore, numerous attempts have been made to tune the spectrum wavelength over a wide range by changing the composition and local crystal structure of the phosphors (Figure 1). For example,  $\text{Eu}^{2+}$  dopant ions in  $\text{SrAl}_2\text{O}_4$  and  $\text{Sr}_4\text{Al}_{14}\text{O}_{25}$  are known to generate different emission wavelengths owing to their different crystalline structures (orthorhombic for  $\text{Sr}_4\text{Al}_{14}\text{O}_{25}$  and monoclinic for  $\text{SrAl}_2\text{O}_4$ ) [44,58,59]. Kim et al. synthesized  $\text{SrAl}_2\text{O}_4:\text{Eu}^{2+},\text{Dy}^{3+}$  and  $\text{Sr}_4\text{Al}_{14}\text{O}_{25}:\text{Eu}^{2+},\text{Dy}^{3+}$  as green and blue phosphors, respectively, by taking advantage of the different emission wavelengths [14].

Moreover, a new class of  $\text{Eu}^{2+}$ -doped  $\text{Sr}_4\text{Al}_2\text{O}_7$  phosphors was recently reported to exhibit a longer wavelength relative to that of  $\text{SrAl}_2\text{O}_4:\text{Eu}^{2+}$  [31]. Zhang et al. also reported that the emission maximum shifted to a longer wavelength when the Al/Sr ratio increased in  $\text{Eu}^{2+}$ -doped strontium aluminate phosphors [51]. Such spectral shifts in different host materials have been thoroughly explored with computational tools at the atomic and molecular levels using quantum mechanical methods, such as the density functional theory (DFT) and Hartree–Fock (HF) method. Theoretical investigations have indicated that the 4f–5d transition energy of lanthanides becomes redshifted after doping into the host lattice because it can affect the difference in energies of the lowest 4f<sup>n</sup> and the first 4f<sup>n-1</sup>d levels in the lanthanide dopants [26]. Three important factors are thought to determine the spectroscopic redshift of lanthanide ions in host materials: centroid shift, crystal field splitting, and ligand polarization [23]. First, the centroid shift of the 5d orbital can be explained using the nephelauxetic effect. Given that the covalency between the luminescent center and its neighboring anions is proportional to the nephelauxetic effect, the centroid shift is expected to be in the  $\text{F}^- < \text{Cl}^- < \text{Br}^- < \text{I}^- < \text{O}^{2-} < \text{S}^{2-}$  order. Next, the type of the coordination polyhedron of anions around the luminescent center is known to strongly affect the highly susceptible nature of the 5d orbitals; this is referred to as crystal field splitting. Therefore, this effect is considered to play a crucial role in determining the spectral redshift of lanthanides in the host materials. Finally, ligand polarization was proposed as an important factor for determining the spectroscopic redshift [60]. The emission wavelengths of  $\text{SrO}:\text{Eu}^{2+}$  and  $\text{Sr}_2\text{SiO}_4:\text{Eu}^{2+}$  phosphors, which cannot be explained using the centroid shift, can be elucidated using ligand polarization.

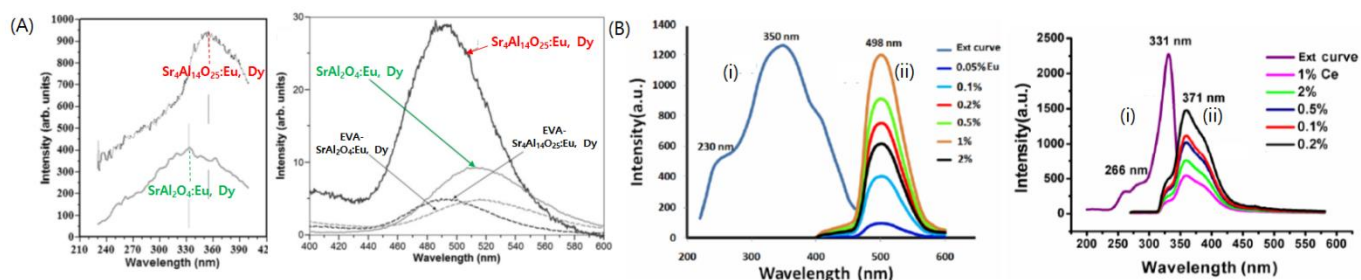


**Figure 1.** Photoluminescence spectra for lanthanide doped strontium aluminate phosphors (A) Photoluminescence excitation (left) and emission (right) spectra for  $\text{SrAl}_2\text{O}_4:\text{Eu}^{2+},\text{Dy}^{3+}$  and  $\text{Sr}_4\text{Al}_{14}\text{O}_{25}:\text{Eu}^{2+},\text{Dy}^{3+}$ . Reprinted from [61] with permission from Elsevier. (B) Photoluminescence excitation (i) and emission (ii) spectra for  $\text{SrAl}_2\text{O}_4:\text{Eu}^{2+}$  (left) and  $\text{SrAl}_2\text{O}_4:\text{Ce}^{3+}$  (right). Adapted from [30] under Creative Commons Attribution (CC BY) license.

## 2.2. Synthesis of Strontium Aluminate Phosphors

Various methods have been employed for the synthesis of lanthanide-doped strontium aluminate phosphors, such as sol–gel, solid-state reaction, combustion, microwave sintering, precursor, and coprecipitation. The selection of the appropriate synthesis method is crucial because it can significantly affect the quality of the luminescent material.

Among these methods, solid-state reactions have been extensively used for phosphor synthesis. This method is based on the chemical reactions between precursors in a powder form at high temperatures (1300–1600 °C). During this process,  $\text{Eu}^{3+}$  is reduced to  $\text{Eu}^{2+}$  in a reducing atmosphere; various reductants, such as  $\text{H}_2 + \text{N}_2$ , HI, and  $\text{NH}_4\text{I}$ , are employed to facilitate this. The reductive atmosphere is crucial for avoiding sample decomposition or oxidization. Moreover, fluxing agents such as  $\text{H}_3\text{BO}_3$  or LiF are often employed during this process to facilitate grain formation and crystal growth [62]. This method is popular in industrial settings because it is a conventional and robust method for the preparation of lanthanide-activated phosphors. For example, the solid-state reaction method was employed by Kim et al. and He et al. to synthesize  $\text{SrAl}_2\text{O}_4:\text{Eu}^{2+}, \text{Dy}^{3+}$  and  $\text{Eu}^{2+}$ -doped  $\text{Sr}_4\text{Al}_2\text{O}_7$  phosphors, respectively [12,48]. This method does not produce toxic or unwanted wastes and is, therefore, considered environmentally friendly. However, it is relatively difficult to accurately control and uniformly mix the individual components via chemical reactions in solid phases, in contrast to those in liquid phases. Additionally, the high-temperature sintering employed in this process for a relatively long reaction time often results in poor homogeneity in the product. Therefore, to avoid the formation of inhomogeneous grain boundaries, protocols involving pretreatment of the starting precursors at low temperatures (500–600 °C) followed by sintering at high temperatures (>1000 °C) have been employed [63,64].

The sol-gel method has been considered an attractive and straightforward alternative to the solid-state reaction method. In this process, solid particles suspended in a liquid (“sol”) are transformed into a three-dimensional network throughout the liquid (“gel”) via polycondensation reactions of molecular precursors. This process is conducted at a relatively low reaction temperature (~950 °C) to facilitate the uniform mixing of the starting materials and the formation of homogeneous products compared to those obtained from the solid-state reaction. This method has been employed for the synthesis of various mixed-metal oxides, nanomaterials, and organic–inorganic hybrids over the last few decades. Both nonaqueous and aqueous sol-gel methods have been employed. The aqueous sol-gel process is considered better than the nonaqueous process because the former facilitates the formation of a homogeneous solid-state structure at the atomic level, which is based on the chemical interactions among the precursor species in the mixture [65]. Misevicius et al. employed this concept in using the aqueous sol-gel approach for the synthesis of various Ce-doped strontium aluminates using glycolate intermediates, such as  $\text{SrAl}_2\text{O}_4$ ,  $\text{Sr}_3\text{Al}_2\text{O}_6$ , and  $\text{Sr}_4\text{Al}_4\text{O}_{10}$  [52].

Although the sol-gel technique can be successfully employed at a relatively low temperature (950 °C), both the solid-state reaction and sol-gel methods have unavoidable limitations, such as the extreme temperatures for long durations. To overcome them, the combustion method has been used as a promising technique for the synthesis of aluminate phosphors. This method is based on a self-sustaining exothermic redox reaction between the materials present in the starting mixture, which includes metal nitrates and urea as the oxidant and fuel, respectively. The reaction between the nitrates and fuel results in the formation of crystalline phases using the sufficient heat even at low temperatures. High levels of chemical homogeneity are also obtained because of their dissolution in the aqueous solution; this is followed by a uniform distribution of luminescent centers. In the  $\text{Eu}^{2+}$ -doped phosphors,  $\text{Eu}^{3+}$  ions are reduced to  $\text{Eu}^{2+}$  by the gas released in this process [66]. This method has been extensively used to prepare various oxide materials, because it is relatively easy to avoid washing, filtration, and drying. This method is also preferred for the preparation of oxide materials at low temperatures. It is safe and efficient with respect to energy conservation because this process can be completed in only a few minutes (~5 min) at low temperatures. This reasoning was employed by Singh et al. to prepare the  $\text{SrAl}_{12}\text{O}_{19}:\text{Eu}^{2+}$  phosphor via the combustion method, which was found to conserve time, energy, and costs [49]. The combustion method has also been used to prepare dysprosium-doped strontium aluminate phosphors ( $\text{SrAl}_2\text{O}_4:\text{Dy}^{3+}$ ) and  $\text{SrAl}_2\text{O}_4:\text{Eu}^{2+}, \text{Nd}^{3+}$  phosphors [27,42].

Finally, the precursor method involves the thermal decomposition of a single molecular precursor at high temperatures, which leads to the formation of nanophosphors. In this method, selection of the appropriate precursor is crucial for the synthesis of pure mixed oxides. Therefore, multimetallic complex compounds are typically preferred in this approach because they allow an intimate molecular-level contact of the metal ions. The selection of the appropriate complexation agent is also important for facilitating the production of complex compounds at low temperatures that can decompose easily. The molar ratios of the chemical elements in the final product can be easily controlled by changing the precursor concentration. This method is considered economically viable compared to other phosphor synthesis methods. The precursor method has also been used to prepare Tb<sup>3+</sup>-doped alkaline earth aluminates, such as SrAl<sub>2</sub>O<sub>4</sub>:Tb<sup>3+</sup>; scanning electron microscopy (SEM) analysis on these phosphors revealed that a homogeneous microstructure with a fine particle size was obtained [33].

In most of the aforementioned phosphor synthesis methods (solid-state reaction, sol-gel processing, combustion), crystalline materials with an average particle size of several tens of micrometers are produced. Therefore, to prepare nanometer-sized phosphors, post-treatment of the bulk phosphors that involves grinding of the large phosphor particles is necessary. Therefore, the particle size of the phosphor can be controlled. However, this process has several disadvantages, such as the unexpected oxidization of a few Eu<sup>2+</sup> ions into inactive Eu<sup>3+</sup> ions in the host lattice during the particle size reduction. In addition, the luminescent performance of the phosphors is degraded because of changes in the local coordination environment, such as crystallinity and lattice microstructure, around the dopants in the strontium aluminate hosts. For instance, Havasi et al. demonstrated the use of the ball-milling method for the production of submicrometer-sized particles of rare-earth-metal-doped strontium aluminate phosphors [50]. A comparative study of the mechanical stress resistance of various phosphors was used to observe the significant loss of long-persistent luminescence. However, this method is acceptable for use in industrial settings, although the elucidation of mechanisms involved and the feasibility of thermal restoration of the performance remain unclear. In addition to phosphor milling, various nanoengineering methods have been developed to synthesize ultrafine nanophosphors. For example, the use of surfactants or chelating reagents in hydro (solvo) thermal or microwave-assisted reactions was found to be effective for controlling the growth of the phosphor size [23]. In addition, laser ablation, template-directed synthesis, and microemulsion routes have been attempted to control the size and morphology of the phosphors [67].

### 2.3. Codoping of Strontium Aluminate Phosphors with Various Trivalent Lanthanide Ions

The luminescent properties of lanthanide-doped strontium aluminate phosphors can be further improved by codoping with other trivalent lanthanide ions as coactivators (such as Ln<sup>3+</sup>). The codoping of SrAl<sub>2</sub>O<sub>4</sub>:Eu<sup>2+</sup> with Dy<sup>3+</sup> resulted in a phosphor with an improved afterglow lifetime, intensity, and chemical stability compared to those of the SrAl<sub>2</sub>O<sub>4</sub>:Eu<sup>2+</sup> phosphors [68]. In particular, the afterglow of SrAl<sub>2</sub>O<sub>4</sub>:Eu<sup>2+</sup>,Dy<sup>3+</sup> was noted to last for over 10 h after exposure to illumination, and showcased a >10-fold increase in the initial intensity, making it an optimal material with persistent luminescence [43]. Interestingly, the position and shape of the luminescence emission band do not change, and the characteristic luminescence of Dy<sup>3+</sup> is rarely observed in this coactivator-doped compound [56]. The direct excitation of Dy<sup>3+</sup> or the energy transfer from Eu<sup>2+</sup> to Dy<sup>3+</sup> is noted to be negligible during the afterglow process. This implies that the luminescence center in these compounds does not change upon the incorporation of Dy<sup>3+</sup>, and it remains centered at Eu<sup>2+</sup>. Although the Dy<sup>3+</sup> profiles are often observed only in the radioluminescence spectrum, they are likely to be hidden because of their weak intensities under the bright emission profiles of Eu<sup>2+</sup> in most cases [41,69]. Other lanthanide ions such as Nd<sup>3+</sup> and Tm<sup>3+</sup> have also been employed as coactivators and were noted to exhibit similarly strong emission bands from the Eu<sup>2+</sup> luminescence center without their characteristic photoluminescence [44,70].

The effect of coactivator concentration on the afterglow has also been investigated. Kim et al. reported that the  $\text{SrAl}_2\text{O}_4:\text{Eu}^{2+},\text{Dy}^{3+}$  phosphor exhibited the strongest persistent luminescence at a  $\text{Dy}^{3+}/\text{Eu}^{2+}$  ratio of  $\sim 2.4$  [12]; the afterglow luminance intensity was found to decrease as the  $\text{Dy}^{3+}/\text{Eu}^{2+}$  ratio surpassed  $\sim 2.4$ , possibly because of the formation of the  $\text{DyAlO}_3$  by-product from residual and insoluble  $\text{Dy}^{3+}$  ions. The afterglow intensity from  $\text{Eu}^{2+}$  has been observed to increase as the dopant and codopant concentration increased [32]; the afterglow intensity was noted to decrease beyond its maximum value because of the concentration quenching effect, similar to that in the study discussed previously [12]. Such concentration effects involving the dopant and codopant can be explained by their distances.

Although codoping with lanthanide ions is known to significantly improve the luminescence, the exact role of  $\text{Dy}^{3+}$  in host materials remains unclear. The general understanding of codoping with lanthanide ions involves their contribution to the trapping centers of the material. For example,  $\text{Dy}^{3+}$  ions doped in the  $\text{Sr}^{2+}$  sites have been proposed to act as electron traps [38,70–72]. This is because the  $\text{Dy}^{3+}$  codopant ions are likely to replace the  $\text{Sr}^{2+}$  ions because of their similar radii and result in a +1 charge incompatibility. In addition, the concentration ratio of  $\text{Eu}^{2+}$  and  $\text{Eu}^{3+}$  after the chemical reduction process can be modified via the codopant ions because they can stabilize the Eu valences in the phosphors [73]. Similarly,  $\text{Dy}^{3+}$  ions are expected to modify the environment of  $\text{Eu}^{2+}$  ions in the  $\text{SrAl}_2\text{O}_4$  host materials. Other possibilities include the trapping of a hole by  $\text{Dy}^{3+}$  or the attraction of other defects for charge compensation [56].

#### 2.4. Mechanisms of Long-Persistent Luminescence from Lanthanide-Doped Strontium Aluminate Phosphors

Several models have been suggested to elucidate the persistent luminescence of codoped  $\text{SrAl}_2\text{O}_4:\text{Eu}^{2+},\text{Dy}^{3+}$  (Figure 2). The differences in these models arise from the assumptions regarding the charge carriers (holes or electrons), pathways of the charge carriers (valence band, conduction band, trapping centers), nature of trapping centers (intrinsic defects or codopants), and excitation mechanism of luminescence. Although the elucidation of persistent luminescence mechanisms in codoped  $\text{SrAl}_2\text{O}_4:\text{Eu}^{2+},\text{Dy}^{3+}$  remains incomplete, the general background in all these models involves the generation of migrating charge carriers during excitation and subsequent localization in trapping centers. The important models that try to explain the mechanism behind the long afterglow in the codoped  $\text{SrAl}_2\text{O}_4:\text{Eu}^{2+},\text{Dy}^{3+}$  phosphor are discussed in this section.

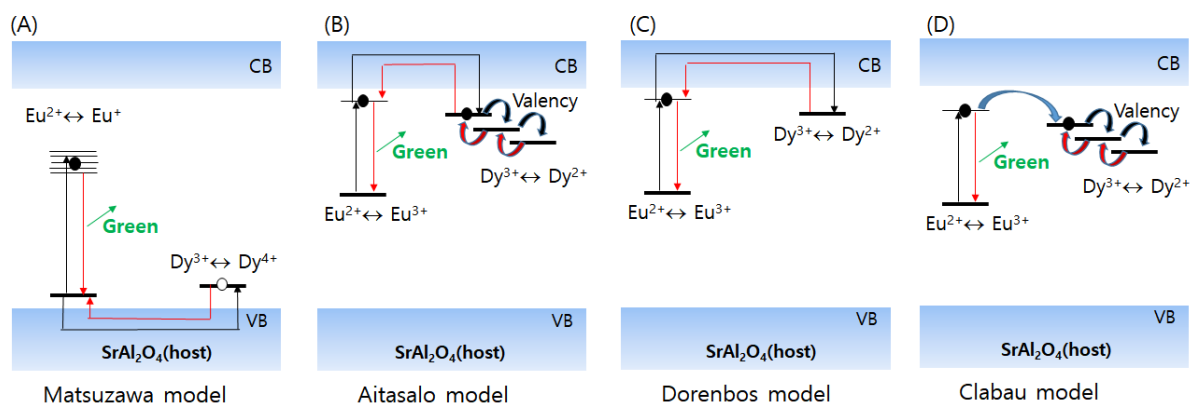


**Figure 2.** The (A) Matsuzawa, (B) Aitasalo, (C) Dorenbos, (D) Clabau models for the photoluminescence of  $\text{SrAl}_2\text{O}_4:\text{Eu}^{2+},\text{Dy}^{3+}$ .

The first of these models was proposed by Matsuzawa et al. [5]. Briefly, the model involves the generation of a hole during  $\text{Eu}^{2+}$  excitation and subsequent  $\text{Eu}^+$  formation, subsequent release and migration of the hole to  $\text{Eu}^+$  through the valence band at a high temperature, and generation of  $\text{Eu}^{2+}$  in the excited state; a photon is also subsequently

released from the excited  $\text{Eu}^{2+}$ . In this model, Dy acts as a hole-trapping center by localizing the holes released from  $\text{Eu}^{2+}$ , and it facilitates the conversion of  $\text{Dy}^{3+}$  to  $\text{Dy}^{4+}$ . Therefore, the hole release and migration from the trapping centers to  $\text{Eu}^+$  is crucial to determining the afterglow. However, the main problem in this model involves the energetically unfavorable formation of  $\text{Eu}^+$ .

To overcome this limitation, Aitasalo et al. proposed a new model for codoped  $\text{SrAl}_2\text{O}_4:\text{Eu}^{2+},\text{Dy}^{3+}$  [43,74,75]. In this model, the possibility of  $\text{Eu}^+$  formation is excluded, and the formation of electron traps and migration of electrons is considered instead of hole traps. Trivalent rare-earth codopants play an important role in trapping electrons at the defect level in this model. As shown in Figure 2B, electrons from the  $\text{Eu}^{2+}$  excited state are thermally promoted to the conduction band and are eventually trapped on defect levels, such as oxygen vacancies, trivalent rare-earth ions, cation vacancies, and interstitial ions. The charge carriers subsequently migrate back to the luminescence center,  $\text{Eu}^{2+}$ , which is followed by the characteristic luminescence of the transition of  $\text{Eu}^{2+}$  to the ground state. Studies involving X-ray absorption near-edge structure (XANES) and extended X-ray absorption fine structure (EXAFS) analyses have verified this model by confirming the accumulation of  $\text{Eu}^{3+}$  during excitation. The  $\text{Eu}^{2+}/\text{Eu}^{3+}$  oxidation has also been observed in XANES measurements of  $\text{SrAl}_2\text{O}_4:\text{Eu}^{2+},\text{Dy}^{3+}$ , which support this model [46]. Qiu et al. suggested that such trapping and detrapping processes from the defect levels can be repetitive [38].

Dorenbos et al. proposed a similar model [72], in which the dopant and codopant energy levels in the bandgap of the  $\text{SrAl}_2\text{O}_4$  host material were estimated. In particular, the energy levels of  $\text{Eu}^{3+}$  and  $\text{Dy}^{3+}$  were presumed to be positioned immediately below the bottom of the conduction band, and  $\sim 0.9$  eV below the bottom of the conduction band, respectively. Because the difference between these energy levels and that of the conduction band is small, thermal ionization is likely to occur at room temperature. The electron that migrates through the conduction band is eventually trapped by  $\text{Dy}^{3+}$ , which is followed by recharging to  $\text{Dy}^{2+}$ . Subsequently, the electron can be thermally released from  $\text{Dy}^{2+}$  and migrates to the excited  $\text{Eu}^{2+}$  center, which eventually leads to the photon emission. The main difference between this model and the Aitasalo model is the type of electron trap discussed. The model presented by Dorenbos et al. only considers trivalent rare-earth ions, whereas that by Aitasalo et al. suggests various kinds of defects, such as oxygen vacancies and trivalent rare-earth ions [43,74,75].

Clabau et al. proposed a new model that involved the formation of  $\text{Eu}^{3+}$  and electron migration, in a manner similar to that discussed in the abovementioned models [54]. Based on results from EPR experiments, the ionization of  $\text{Eu}^{2+}$  to  $\text{Eu}^{3+}$  was assumed to occur after excitation by UV irradiation. The main difference between this and the previous models involves the direct migration of electrons between the luminescence and trapping centers and not via the conduction band. This can occur if the energy levels of  $\text{Eu}^{3+}$  and trapping centers are located close to each other.

Broadly speaking, all the aforementioned models describe the generation of charge carriers during excitation, and their subsequent localization in trapping centers postmigration. The charge carrier is subsequently released from the trapping centers and eventually recombined with the excited luminescent center. The model that best represents the persistent luminescence in  $\text{SrAl}_2\text{O}_4:\text{Eu}^{2+},\text{Dy}^{3+}$  is likely to involve the creation of  $\text{Eu}^{3+}$  and the radiative  $\text{Eu}^{2+}$  transition to the ground state. Moreover, there may be several trapping centers present in the phosphor, although their exact nature remains unclear.

The use of multiple codopants has also been attempted because of the effectiveness of codoping for the enhancement of the luminescence of  $\text{Eu}^{2+}$ . Song et al. and Li et al. employed  $\text{Tb}^{3+}$  and  $\text{Er}^{3+}$  as additional codopants in  $\text{Sr}_4\text{Al}_{14}\text{O}_{25}:\text{Eu}^{2+},\text{Dy}^{3+}$ , respectively [45,47]. In addition, Havasi et al. demonstrated the photoluminescence properties of  $\text{Sr}_4\text{Al}_{14}\text{O}_{25}:\text{Eu}^{2+},\text{Dy}^{3+},\text{Ho}^{3+}$ , which was synthesized using  $\text{Dy}^{3+}$  and  $\text{Ho}^{3+}$  as additional codopants [50]. During sample preparation in this study,  $\text{Dy}^{3+}$  in  $\text{Sr}_4\text{Al}_{14}\text{O}_{25}:\text{Eu}^{2+}/\text{Dy}^{3+}$  was presumed to be partially substituted with  $\text{Ho}^{3+}$ , which remarkably increased the

photoluminescence intensity and shifted the main emission peaks. This was explained via the effect of  $Dy^{3+}/Ho^{3+}$  on the trapping/de-trapping and energy transfer processes in this phosphor [76].

### 3. Calcium Aluminate Phosphors

Calcium aluminate is also considered as a useful host matrix material for phosphors (Table 2). Similar to strontium aluminate, calcium aluminate has been known to exhibit a bright emission over a wide visible range and a high energy efficiency, quenching temperature, and chemical stability. In addition, its high toughness, strength, and high-temperature resistance facilitate its use as cement materials [77]. In particular, calcium aluminates have been applied as dental cements and bone grafts because of their bioactive, biocompatible, physical, and mechanical properties.

**Table 2.** Comparison of reported studies for the synthesis of lanthanide-doped calcium aluminate phosphors.

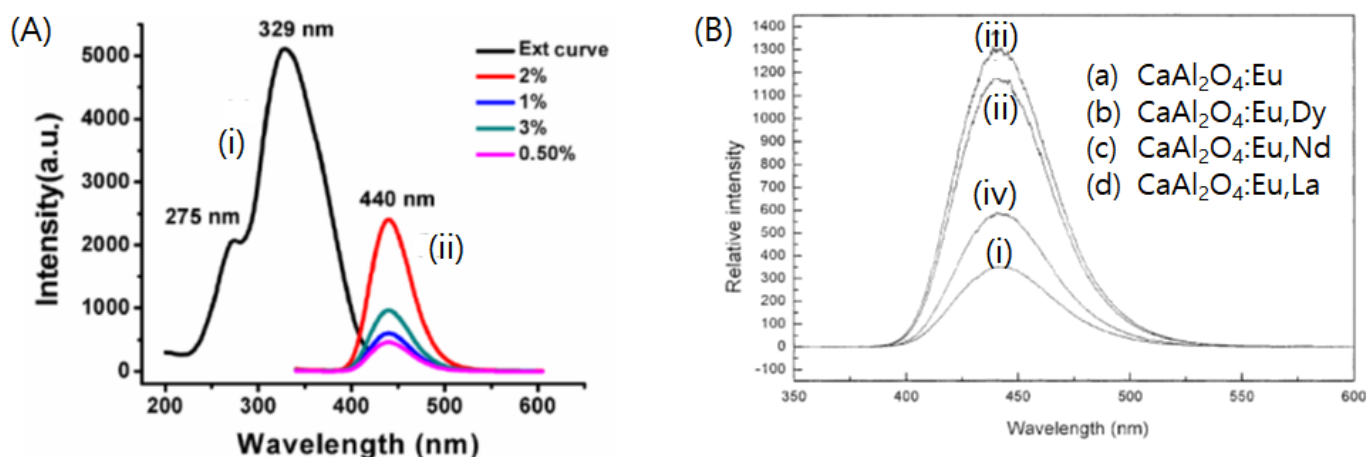
Host Material	Activator	Co-Activator	Synthesis Method	Color or $\lambda$	Remarks	Ref
CaAl <sub>2</sub> O <sub>4</sub>	Eu <sup>2+</sup>	-	Solid-state reaction (1250–1300 °C)	Blue ( $\lambda_{em} = 440$ nm)	The new mechanism was proposed, which involves the excited state absorption of two 530 nm photons via deep traps followed by trapping of electrons in shallow traps.	[75]
		-	Solid-state reaction (1300 °C)	Blue ( $\lambda_{em} = 442$ nm)	Good morphology and the best luminous intensity could be gained when H <sub>3</sub> BO <sub>3</sub> mass ratio was 0.5 wt%.	[78]
	Tb <sup>3+</sup>	-	Precursor route via the thermal decomposition of tartarate compounds	$\lambda_{em} = 542$ nm	They demonstrated that the precursor method via the thermal decomposition of multimetallic tartarate compounds is a quick, simple and inexpensive way for the preparation of alkaline-earth aluminate powder.	[33]
	Pr <sup>2+</sup>	-	Sol–gel method	$\lambda_{em} = 390$ nm, 520 nm, 790 nm	The interlinked small granular structured particles finally formed bigger particles.	[9]
	Eu <sup>2+</sup> or Nd <sup>3+</sup>	-	Solid-state reaction (1000 °C)	-	A systematic study of the structures of the alkaline earth aluminates using a combination of synchrotron X-ray and neutron powder diffraction.	[13]
	La <sup>3+</sup> or Tb <sup>3+</sup>	-	Sol–gel method	Blue-green $\lambda_{em} = 395$ nm, 535 nm	Emission peak position is not altered by doping with La <sup>3+</sup> , Tb <sup>3+</sup> , but variation in the intensity is observed.	[79]
	Eu <sup>2+</sup> or Ce <sup>3+</sup>	-	Combustion method (600 °C)	Eu <sup>2+</sup> : $\lambda_{ex} = 275, 329$ nm, $\lambda_{em} = 440$ nm Ce <sup>3+</sup> : $\lambda_{ex} = 247, 300$ nm, $\lambda_{em} = 370$ nm	Experimental results matched with the predictions of Dorenbos' model.	[30]

Table 2. Cont.

Host Material	Activator	Co-Activator	Synthesis Method	Color or $\lambda$	Remarks	Ref	
CaAl <sub>2</sub> O <sub>4</sub>	Eu <sup>2+</sup>	Nd <sup>3+</sup>	Floating zone technique	Blue ( $\lambda_{em} = 450$ nm)	The intensities and the persistent times of the phosphorescences are found to depend on the growth atmosphere.	[34]	
			Laser-heated pedestal growth method	Blue ( $\lambda_{em} = 445$ nm)	It was found that multiple trapping centers are involved in the phosphorescence dynamic processes, which is responsible for the long persistence.	[35]	
			Combustion method	Blue ( $\lambda_{em} = 440$ nm)	Eu <sup>2+</sup> , Nd <sup>3+</sup> co-doped calcium aluminate showed bright phosphorescence with a long duration.	[80]	
			Solid-state reaction (1300 °C)	Blue ( $\lambda_{em} = 442$ nm)	The composition of the activator Eu <sup>2+</sup> and the co-activator Nd <sup>3+</sup> , the doping conditions with alkaline earth metals, alkali metals, and Si were optimized.	[81]	
			Combustion method (550 °C)	Blue ( $\lambda_{ex} = 355$ nm, $\lambda_{em} = 492$ nm)	Nd <sup>3+</sup> trap levels can be thought of as the lanthanide element that causes long phosphorescence at room temperature.	[42]	
	Eu <sup>2+</sup>	Dy <sup>3+</sup>	Solid-state reaction (900–1350 °C)	$\lambda_{em} = 445$ nm	The depth of Dy <sup>3+</sup> trap levels is in the order of BaAl <sub>2</sub> O <sub>4</sub> host > CaAl <sub>2</sub> O <sub>4</sub> host > SrAl <sub>2</sub> O <sub>4</sub> host.	[36]	
			Combustion method (500 °C)	$\lambda_{em} = 449$ nm	They found that the monoclinic crystal structures of both CaAl <sub>2</sub> O <sub>4</sub> and SrAl <sub>2</sub> O <sub>4</sub> are more appropriate in creating the traps, which is directly related to the long afterglow phenomena.	[39]	
			Na <sup>+</sup>	Solid-state reaction followed by ball-milling	$\lambda_{em} = 440$ nm,	This report presents the factors affecting the luminescence properties of the Eu <sup>2+</sup> -, R <sup>3+</sup> -doped SrAl <sub>2</sub> O <sub>4</sub> .	[43]
			La <sup>3+</sup>	Combustion method (600 °C)	blue-purple ( $\lambda_{em} = 440$ nm)	They proposed that phosphor samples obtain a persistent luminescence with the aid of the energy transfer at the trap level.	[38]
			Dy <sup>3+</sup> , Nd <sup>3+</sup> , La <sup>3+</sup>	Solid-state reaction (1380 °C)	Blue ( $\lambda_{em} = 440$ nm)	Both initial brightness and persistent afterglow time of CaAl <sub>2</sub> O <sub>4</sub> : Eu <sup>2+</sup> , Nd <sup>3+</sup> is better than those of CaAl <sub>2</sub> O <sub>4</sub> : Eu <sup>2+</sup> , Dy <sup>3+</sup> , and CaAl <sub>2</sub> O <sub>4</sub> : Eu <sup>2+</sup> , La <sup>3+</sup> .	[82]
La <sup>3+</sup> –Lu <sup>3+</sup> , Y <sup>3+</sup> ; except Pm <sup>3+</sup> , Eu <sup>3+</sup>			Solid-state reaction (1250–1300 °C)	Green ( $\lambda_{em} = 440$ nm)	The co-doping by Dy <sup>3+</sup> intensifies the luminescence by an order of magnitude, whereas the easily reducible rare earths, such as Sm <sup>3+</sup> and Yb <sup>3+</sup> , suppressed both the afterglow and the thermoluminescence.	[46]	

### 3.1. Calcium Aluminate Phosphors with Diverse Colors

Calcium aluminates belong to the spinel group of minerals, similar to the other alkaline earth aluminates. The typical chemical representation of calcium aluminate is  $\text{CaAl}_2\text{O}_4$ , and it exists in the monoclinic or orthorhombic forms [83]. As discussed earlier, the host crystal structure and activator are the important factors for determining the main emission peaks of aluminate-based phosphors. For example,  $\text{CaAl}_2\text{O}_4:\text{Eu}^{2+}$  is known to exhibit blue light emission, which corresponds to a shorter emission wavelength in the  $\text{SrAl}_2\text{O}_4:\text{Eu}^{2+}$  system. Among the various lanthanide-doped calcium aluminate phosphors,  $\text{CaAl}_2\text{O}_4:\text{Eu}^{2+}$  is extensively used as a phosphor material (Figure 3). As an emission center,  $\text{Eu}^{2+}$  is known to emit blue light via the  $4f^65d \rightarrow 4f^7$  transition, whose peak is located at  $\sim 442$  nm [78]. Its absorption is observed at near-UV light, which is similar to that via LED chips. Although there are fewer studies on  $\text{CaAl}_2\text{O}_4$  phosphors than those on  $\text{SrAl}_2\text{O}_4$ , the former has attracted considerable recent interest as a luminescent host owing to its high color purity and stability; it also meets the high-efficiency-based requirements for novel blue-emitting phosphors [84].



**Figure 3.** Photoluminescence spectra for lanthanide doped calcium aluminate phosphors (A) Photoluminescence excitation (i) and emission (ii) spectra for  $\text{CaAl}_2\text{O}_4:\text{Eu}^{2+}$ . Adapted from Ref. [30] under Creative Commons Attribution (CC BY) license. (B) Emission spectra of (i)  $\text{CaAl}_2\text{O}_4:\text{Eu}^{2+}$ , (ii)  $\text{CaAl}_2\text{O}_4:\text{Eu}^{2+},\text{Dy}^{3+}$ , (iii)  $\text{CaAl}_2\text{O}_4:\text{Eu}^{2+},\text{Nd}^{3+}$ , (iv)  $\text{CaAl}_2\text{O}_4:\text{Eu}^{2+},\text{La}^{3+}$ . Adapted with permission from [82]. Copyright Elsevier, 2003.

Several activators have been experimented as dopants for  $\text{CaAl}_2\text{O}_4$ . For example,  $\text{Tb}^{3+}$ , which has been doped into  $\text{CaAl}_2\text{O}_4$  in several studies, can substitute a  $\text{Ca}^{2+}$  ion as  $\text{Eu}^{2+}$ , which is followed by the formation of a charge defect [85];  $\text{CaAl}_2\text{O}_4:\text{Tb}^{3+}$  was found to exhibit an emission wavelength of 545 nm, which corresponded to the f-f transitions of  $\text{Tb}^{3+}$ .  $\text{La}^{3+}$ -doped  $\text{CaAl}_2\text{O}_4$  synthesized via the sol-gel method exhibited an emission peak at 395 nm in the blue region [79]; its emission band intensity was observed to be stronger than that of  $\text{CaAl}_2\text{O}_4:\text{Tb}^{3+}$ . The particle sizes of  $\text{CaAl}_2\text{O}_4:\text{La}^{3+}$  and  $\text{CaAl}_2\text{O}_4:\text{Tb}^{3+}$  were obtained as 27 nm and 31 nm, respectively, and both had no effect on the phase composition of  $\text{CaAl}_2\text{O}_4$  [79]. Additionally, several studies have attempted the  $\text{Ce}^{3+}$  ion doping of  $\text{CaAl}_2\text{O}_4$  and have resulted in a much shorter emission wavelength (330–350 nm). This emission band corresponds to the  $5d-4f$  transitions of  $\text{Ce}^{3+}$  ions. The broad emission band was found to be remarkably intense because of the transition being parity-allowed [30]. Nonlanthanide ions, such as Mn, have also been employed as activators in  $\text{CaAl}_2\text{O}_4$ . Mn-doped aluminate phosphors synthesized via the combustion process were found to exhibit red emission from the  $\text{Mn}^{4+}$  ions [86]; Mn ions were noted to exist in the  $\text{CaAl}_2\text{O}_4$  host material in both  $\text{Mn}^{2+}$  and  $\text{Mn}^{4+}$  states; they also occupied distorted lattice sites in the host matrix.

### 3.2. Codoping of Calcium Aluminate Phosphors with Various Trivalent Lanthanide Ions

Similar to strontium aluminate phosphors, codoping of  $\text{CaAl}_2\text{O}_4$  phosphor materials with various trivalent lanthanide ions has been attempted to improve their luminescence properties. Lin et al. suggested that the incorporation of  $\text{Dy}^{3+}$ ,  $\text{Nd}^{3+}$ , and  $\text{La}^{3+}$  can possibly enhance the brightness and persistent afterglow time [82]. Regardless of the type of codopant ions used, the excitation and emission of these three phosphors resulted in spectra that were similar in shape to those of the  $\text{CaAl}_2\text{O}_4:\text{Eu}^{2+}$  phosphor, which corresponded to the  $4f^7-4f^65d$  inter-configuration transitions of  $\text{Eu}^{2+}$  ions. Among these phosphors, the afterglow from  $\text{CaAl}_2\text{O}_4:\text{Eu}^{2+},\text{Nd}^{3+}$  was found to be the brightest and with the longest duration.

The  $\text{CaAl}_2\text{O}_4:\text{Eu}^{2+},\text{Nd}^{3+}$  phosphor has, therefore, been extensively investigated. Zhao et al. investigated the UV-excited luminescence of  $\text{CaAl}_2\text{O}_4:\text{Eu}^{2+},\text{Nd}^{3+}$  and observed a broad band in the blue region ( $\lambda_{\text{max}} = 440$  nm) that arose from the  $5d-4f$  transitions of  $\text{Eu}^{2+}$  [80]. The bright afterglow luminescence was observed for a long duration. This long-persistent luminescence was presumed to result from the trapping–transporting–detrapping of the holes, a process in which  $\text{Nd}^{3+}$  ions behaved as hole traps between the ground and the excited states of the  $\text{Eu}^{2+}$  ion. Kim et al. reported the optimized composition of the  $\text{Eu}^{2+}$  activator and  $\text{Nd}^{3+}$  coactivator for  $\text{CaAl}_2\text{O}_4$  [81]. The introduction of  $\text{Nd}^{3+}$  into the  $\text{CaAl}_2\text{O}_4:\text{Eu}^{2+}$  system was found to significantly boost its phosphorescence intensity and lifetime, similar to that of  $\text{Dy}^{3+}$  doping in the  $\text{SrAl}_2\text{O}_4:\text{Eu}^{2+}$  system. Composition-based studies on the activator ( $\text{Eu}^{2+}$ ) and coactivator ( $\text{Nd}^{3+}$ ) have revealed that the afterglow intensity and lifetime were strongly affected by the concentrations of  $\text{Eu}^{2+}$  and  $\text{Nd}^{3+}$  in  $\text{CaAl}_2\text{O}_4:\text{Eu}^{2+},\text{Nd}^{3+}$ ; this implies that the optimization of the activator and coactivator concentrations appears to be important for obtaining a high intensity of phosphorescence. The afterglow of phosphors with various concentrations of the activator ( $\text{Eu}^{2+}$ ) and coactivator ( $\text{Nd}^{3+}$ ) were measured, and  $\sim 0.006$  mol of  $\text{Eu}^{2+}$  per mol of  $\text{CaAl}_2\text{O}_4:\text{Eu}^{2+},\text{Nd}^{3+}$ , and an  $\text{Nd}^{3+}/\text{Eu}^{2+}$  ratio of 1 were found to result in a product with the brightest phosphorescence emission for the longest duration. This optimized concentration was noted to be much lower than that of  $\text{Eu}^{2+}$  ( $\sim 0.935$  mol per mol of  $\text{SrAl}_2\text{O}_4:\text{Eu}^{2+},\text{Dy}^{3+}$ ) and  $\text{Dy}^{3+}$  ( $\sim 2.244$  mol per mol of  $\text{SrAl}_2\text{O}_4:\text{Eu}^{2+},\text{Dy}^{3+}$ ) in the green-emitting  $\text{SrAl}_2\text{O}_4:\text{Eu}^{2+},\text{Dy}^{3+}$  phosphor, probably because of their relatively large sizes.

### 3.3. Synthesis of Calcium Aluminate Phosphors

The  $\text{CaAl}_2\text{O}_4:\text{Eu}^{2+}$  phosphors are typically prepared in a manner similar to that for the  $\text{SrAl}_2\text{O}_4:\text{Eu}^{2+}$  phosphors. The high-temperature solid-state reaction is intensively used for the preparation of  $\text{CaAl}_2\text{O}_4:\text{Eu}^{2+}$ ; however, the high calcination temperature and the formation of heterogeneous particles with relatively large microscale sizes limit their applications. Therefore, the various properties of the fluxing agent in the solid-state process have been modified to control the particle size and reduce the sintering temperature. This is attempted because the fluxing agent is presumed to facilitate the incorporation of lanthanide ions in the matrix lattice. For example, the effect of the concentration of  $\text{H}_3\text{BO}_3$  as a fluxing agent on the structure, morphology, and luminescent properties of  $\text{Ca}_{1-x}\text{Al}_2\text{O}_4:\text{xEu}^{2+}$  have been explored by Zeng et al. [78] A comparison of different amounts of  $\text{H}_3\text{BO}_3$  for phosphor synthesis revealed that an  $\text{H}_3\text{BO}_3$  mass ratio of 0.5 wt.% resulted in a product with an adequate morphology without agglomeration and the best luminous intensity among the various samples. Kim et al. also presented a comparative study of varying amounts of  $\text{H}_3\text{BO}_3$  [81], which suggested that 0.25 mol per mol of  $\text{CaAl}_2\text{O}_4:\text{Eu}^{2+},\text{Nd}^{3+}$  resulted in the brightest phosphorescence among the various samples; however, a higher concentration of  $\text{H}_3\text{BO}_3$  was found to produce a hardened final product, which can create difficulties in the subsequent mortar grinding process.

Several alternative methods involving liquid phases, such as sol–gel, combustion, coprecipitation, and microwaves, have been employed for the preparation of  $\text{CaAl}_2\text{O}_4:\text{Eu}^{2+}$ , in a manner similar to that for strontium aluminate phosphors. In the liquid phase, each component can be uniformly mixed and accurately controlled. For example, the sol–gel

process facilitates the homogeneous mixing of the starting materials and synthesis at a relatively low reaction temperature, which results in the formation of homogeneous products with a fine grain size [37,82]. The combustion method is another efficient technique for the preparation of  $\text{CaAl}_2\text{O}_4:\text{Eu}^{2+}$  at a relatively low temperature and is known for being facile, safe, quick, cost-effective, and energy conserving. Zhao et al. reported that the  $\text{CaAl}_2\text{O}_4$  phase was formed at a combustion initiation temperature of  $400\text{ }^\circ\text{C}$  via the combustion method; this method resulted in the formation of persistent luminescent  $\text{CaAl}_2\text{O}_4:\text{Eu}^{2+}$ -based phosphors with bright phosphorescence and a long duration [80].

Several methods have been recently attempted for the preparation of  $\text{Eu}^{2+}$ -doped calcium aluminate phosphors. Jia et al. employed a LASER-heated pedestal growth method to synthesize the  $\text{CaAl}_2\text{O}_4:\text{Eu}^{2+},\text{Nd}^{3+}$  phosphor, which resulted in bright and long-persistent phosphorescence being observed from the final product [35]. Katsumata et al. attempted a loading zone technique to grow a single-crystal  $\text{CaAl}_2\text{O}_4:\text{Eu}^{2+},\text{Nd}^{3+}$  phosphor, and the resulting product exhibited luminescent properties similar to those of the previously reported  $\text{SrAl}_2\text{O}_4:\text{Eu}^{2+},\text{Dy}^{3+}$  phosphor [34].

#### 4. Barium Aluminates

Barium aluminate phosphors are persistent and exhibit high luminescent intensity, long afterglow time, and chemical stability (Table 3). Moreover, their synthesis does not require a reducing atmosphere for dopant reduction [87].

**Table 3.** Comparison of reported studies for the synthesis of lanthanide-doped barium aluminate phosphors.

Host Material	Activator	Co-Activator	Synthesis Method	Color or $\lambda$	Remarks	Ref	
$\text{BaAl}_2\text{O}_4$	$\text{Eu}^{2+}$	-	Solid-state reaction ( $1400\text{ }^\circ\text{C}$ )	$\lambda_{\text{ex}} = 340\text{ nm}$ , $\lambda_{\text{em}} = 498\text{ nm}$	The $\text{Eu}^{3+}$ reduction in $\text{BaAl}_2\text{O}_4:\text{Eu}^{2+}$ prepared in the air could be explained with the charge compensation model.	[8]	
	$\text{Ce}^{3+}$	-	Solid-state reaction ( $900\text{--}1350\text{ }^\circ\text{C}$ )	$\lambda_{\text{ex}} = 357\text{ nm}$ , 335 nm $\lambda_{\text{em}} = 450\text{ nm}$ , 402 nm	Site-selective thermoluminescence spectra showed that traps were close to the corresponding $\text{Ce}^{3+}$ ion.	[88]	
				Combustion method ( $500\text{ }^\circ\text{C}$ )	Red ( $\lambda_{\text{em}} = 705\text{ nm}$ )	The site symmetry of $\text{Cr}^{3+}$ ion in this phosphor is responsible for a distorted octahedron.	[89]
		$\text{Cr}^{3+}$		Hydrothermal route followed by a thermal treatment	-	The dopant $\text{Cr}^{3+}$ cations increased lattice strain and disturbed the crystallites to grow by acting as defects in the barium aluminate structure.	[90]
		$\text{Eu}^{2+}$ or $\text{Nd}^{3+}$	-	Solid-state reaction ( $1000\text{ }^\circ\text{C}$ )	-	A systematic study of the structures of the alkaline earth aluminates using a combination of synchrotron X-ray and neutron powder diffraction.	[13]
		$\text{Eu}^{2+}$ or $\text{Ce}^{3+}$	-	Combustion method ( $600\text{ }^\circ\text{C}$ )	$\text{Eu}^{2+}:\lambda_{\text{ex}} = 270$ , 328, 397 nm, $\lambda_{\text{em}} = 485\text{ nm}$ , $\text{Ce}^{3+}:\lambda_{\text{ex}} = 246$ , 292, 308 nm, $\lambda_{\text{em}} = 386\text{ nm}$	Experimental results matched well with the predictions of Dorenbos' model.	[30]

Table 3. Cont.

Host Material	Activator	Co-Activator	Synthesis Method	Color or $\lambda$	Remarks	Ref	
BaAl <sub>2</sub> O <sub>4</sub>	Eu <sup>2+</sup>	Dy <sup>3+</sup>	Solid-state reaction (900–1350 °C)	$\lambda_{em} = 496$ nm	The depth of Dy <sup>3+</sup> trap levels is in the order of BaAl <sub>2</sub> O <sub>4</sub> host > CaAl <sub>2</sub> O <sub>4</sub> host > SrAl <sub>2</sub> O <sub>4</sub> host.	[36]	
			Solid-state reaction (700–1500 °C)	Green-blue ( $\lambda_{em} = 500$ nm)	The dopant (Eu <sup>2+</sup> ) and co-dopant (Dy <sup>3+</sup> ) concentrations affect the crystallinity and luminescence properties of the materials.	[87]	
			Combustion method (500 °C)	$\lambda_{em} = 450$ nm	The hexagonal structure of BaAl <sub>2</sub> O <sub>4</sub> can only produce shallow traps, resulting in a short afterglow.	[39]	
			Combustion method (400–600 °C) or Solid-state reaction (1500 °C)	$\lambda_{em} = 505$ nm	They found that the method of preparation has a significant effect on the defect structure of the materials.	[87]	
			Combustion synthesis method assisted by microwave irradiation	Blue-green ( $\lambda_{em} = 496$ nm)	The surface of the BaAl <sub>2</sub> O <sub>4</sub> :Eu <sup>2+</sup> ,Dy <sup>3+</sup> powder samples showed lots of voids and pores.	[91]	
			Solid-state reaction (1300 °C)	Green ( $\lambda_{ex} = 355$ nm, $\lambda_{em} = 499$ nm)	The photoluminescence efficiency increased with increasing Eu <sup>2+</sup> concentration until 3 mol% then decreased at higher concentrations due to the concentration quenching effect.	[92]	
		Nd <sup>3+</sup>	-	Combustion method (500 °C)	Blue–green ( $\lambda_{ex} = 340$ nm, $\lambda_{em} = 505$ nm)	The powders exhibited high initial brightness luminescence with subdued long afterglow characteristics.	[93]
				Combustion method (600 °C)	Green-blue ( $\lambda_{em} = 500$ nm)	They proposed that phosphor samples obtain a lifetime of persistent luminescence with the aid of the energy transfer at the trap level.	[38]
				Combustion method (550 °C)	Blue ( $\lambda_{ex} = 355$ nm, $\lambda_{em} = 495$ nm)	Nd <sup>3+</sup> trap levels can be thought of as the lanthanide element that causes long phosphorescence at room temperature.	[42]
				Solid-state reaction (1300 °C)	-	Fibre shaped morphology of the grown material was formed with sharp surface morphology like single crystals.	[94]
		Dy <sup>3+</sup> , Nd <sup>3+</sup> , Gd <sup>3+</sup> , Sm <sup>3+</sup> , Ce <sup>3+</sup> , Er <sup>3+</sup> , Pr <sup>3+</sup> and Tb <sup>3+</sup>	Combustion method (600 °C)	Blue-green ( $\lambda_{em} = 500$ nm)	The highest intensity was observed from Er <sup>3+</sup> co-doping, whereas the longest afterglow was observed from Nd <sup>3+</sup> followed by Dy <sup>3+</sup> co-doping.	[95]	

Barium aluminate ( $\text{BaAl}_2\text{O}_4$ ) has a stuffed tridymite structure that is derived from the  $\text{SiO}_2$   $\beta$ -tridymite structure observed in other alkaline earth aluminates [96]. It has a hexagonal phase, which is different from those of strontium aluminate and calcium aluminate. Barium aluminates exhibit a stable monoclinic phase at low temperatures which are transformed from the hexagonal phase after cooling. Barium aluminate ( $\text{BaAl}_2\text{O}_4$ ) also has a high melting point (1815 °C), and exhibits adequate chemical stability and decent dielectric, pyroelectric, and hydraulic-hardening properties [97]. In its structure, two different sites are available for  $\text{Ba}^{2+}$ : one with a  $C_3$  symmetry and a relatively longer Ba–O distance (2.86–2.87 Å), and the other with a  $C_1$  symmetry and a relatively shorter Ba–O distance (2.69 Å) [94].  $\text{Ba}^{2+}$  has a larger ionic radius (1.34 Å) than that of most other rare-earth ions; this facilitates the straightforward substitution of vacant  $\text{Ba}^{2+}$  sites with lanthanide ions upon doping [88].

#### 4.1. Synthesis of Barium Aluminate Phosphors

Various techniques have been employed to prepare barium aluminate phosphors in a manner similar to those for strontium and calcium aluminate phosphors, such as solid-state reactions, combustion methods, and microwave heating techniques.

The conventional solid-state reaction method has been typically used to successfully prepare barium aluminate phosphors [98]. In contrast to the synthesis of strontium and calcium aluminates, barium aluminate can be synthesized in an oxidizing atmosphere. Peng et al. were the first to report the reduction of  $\text{Eu}^{3+}$  to  $\text{Eu}^{2+}$  in an oxidizing atmosphere (air) via a high-temperature solid-state reaction for doping into an  $\text{AlO}_4$  tetrahedron in the  $\text{BaAl}_2\text{O}_4$  crystal [8]. The tetrahedral  $\text{AlO}_4$  anion groups can form a hard three-dimensional network, which can induce the  $\text{Eu}^{3+}$  reduction even when the barium aluminate phosphors are prepared in air. Therefore, diverse atmospheric conditions such as reducing, weak reducing, and oxidizing atmospheres have been employed to synthesize barium aluminate phosphors. This method is straightforward and does not require expensive or sophisticated equipment; it is also convenient for large-scale industrial production. In addition, it can produce a structurally pure final product with desirable properties, depending on the final sintering temperatures.

Combustion synthesis is another extensively used method for the preparation of barium aluminate phosphors. Annah et al. prepared trivalent lanthanide codoped  $\text{BaAl}_2\text{O}_4:\text{Eu}^{2+}$  phosphors via the combustion method at an initiating temperature of 600 °C and annealing at 1000 °C [95]. The annealing process was found to have no effect on the general properties of the phosphors. Rodrigues et al. also employed this method at similarly low temperatures between 400 and 600 °C; Mothudi et al. synthesized  $\text{BaAl}_2\text{O}_4:\text{Eu}^{2+},\text{Dy}^{3+}$  at a combustion initiation temperature of 500 °C with urea as an organic fuel for combustion [39,99]. The combustion method can be performed at a much lower temperature compared to that in the solid-state reaction, and it is considered to be a simple, time-saving, and cost-effective technique. As previously discussed, it can produce smaller crystals than those obtained from a solid-state reaction. The size of particles produced via the combustion method was found to decrease from 98 nm to 85 nm as the reaction temperature increased from 400 to 600 °C [96]. Another difference between these two methods involves the number of traps produced; one trap is formed in the combustion method, whereas three traps are formed in the solid-state method, which hints at the formation of various defect structures in the materials, depending on the synthesis methods.

$\text{BaAl}_2\text{O}_4$  phosphors have also been synthesized by microwave heating. Zhang et al. successfully synthesized  $\text{BaAl}_2\text{O}_4$  using  $\text{BaCO}_3$  and  $\text{Al}(\text{OH})_3$  powders as raw materials via microwave sintering [100]. These phosphors were characterized by thermogravimetry–differential scanning calorimetry (TG–DSC), X-ray diffraction (XRD), and optical microscopy; this method was found to be feasible for the preparation of persistent luminescence materials of barium aluminates. Although this technique is not employed as frequently as the two previously discussed methods, it has several advantages, such as the

low temperatures and short durations in sintering, a simple and easy setup, cost-effective energy source, and high rate of synthesis.

#### 4.2. Barium Aluminate Phosphors with Various Colors

$\text{Eu}^{2+}$  is the most popular rare-earth element for doping in  $\text{BaAl}_2\text{O}_4$ , similar to that in the alkali metal-based aluminate phosphors [98] (Figure 4).  $\text{BaAl}_2\text{O}_4$  phosphors have been considered for application in plasma display panels (PDPs) and mechanoluminescence (ML) dosimetry owing to their enhanced luminescence intensity, long-lasting duration, and suitable emitting colors via  $\text{Eu}^{2+}$  doping. The peak of the broad excitation spectra is observed at 340 nm, and the emission spectra are present in the blue–green region under vacuum/ultraviolet (VUV) light excitation, which corresponds to the  $5d-4f$  transition of  $\text{Eu}^{2+}$ . The spectral peak does not appear uniform, which implies the occurrence of multiple events at the luminescent centers. Peng et al. reported that  $\text{Eu}^{2+}$  ions can occupy 2 different lattice sites after doping in  $\text{BaAl}_2\text{O}_4$ : the  $\text{Eu}^{2+}$  ion in the first site exhibited a major emission peak at 495 nm, and the  $\text{Eu}^{2+}$  ion in the other exhibited a weak emission peak at 530 nm [8]. The main emission peak is noted to be positioned between the emission peaks of  $\text{SrAl}_2\text{O}_4:\text{Eu}^{2+}$  (528 nm) and  $\text{CaAl}_2\text{O}_4:\text{Eu}^{2+}$  (449 nm), implying that the crystal structure of the host plays a crucial role in determining the main emission peaks of aluminate-based phosphors. In addition, Stefani et al. observed that the relative intensity of the two emission peaks in  $\text{BaAl}_2\text{O}_4:\text{Eu}^{2+}$  can be modified by varying the dopant and codopant concentrations [87]. The intensity of the emission peak at a shorter wavelength was observed to increase as the dopant and codopant concentrations increased, which suggested that  $\text{Eu}^{2+}$  preferentially occupied the  $\text{Ba}^{2+}$  site responsible for longer wavelength emission and subsequently occupied another site corresponding to the shorter wavelength emission. Feilong et al. reported 1 mol.% as the optimal  $\text{Eu}^{2+}$  concentration for the enhancement of luminescent intensity of  $\text{BaAl}_2\text{O}_4$  [91]. Roh et al. also studied the effect of  $\text{Eu}^{2+}$  concentration on the photoluminescence of these phosphors [92]. The photoluminescence efficiency was noted to increase as the  $\text{Eu}^{2+}$  concentration increased up to 3 mol.% and concentrations greater than 3 mol.% quenched the photoluminescence of  $\text{BaAl}_2\text{O}_4:\text{Eu}^{2+}$ .

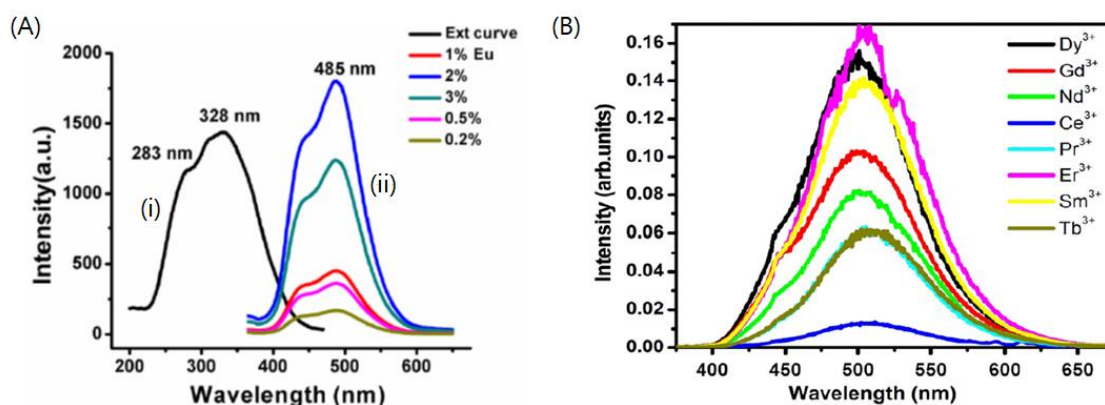


**Figure 4.** Photoluminescence spectra for lanthanide doped barium aluminate phosphors (A) Photoluminescence excitation (i) and emission (ii) spectra for  $\text{BaAl}_2\text{O}_4:\text{Eu}^{2+}$ . Adapted from [30] under Creative Commons Attribution (CC BY) license. (B) Photoluminescence emission spectra of  $\text{BaAl}_2\text{O}_4:\text{Eu}^{2+}$ ,  $\text{Re}^{3+}$  ( $\text{Re} = \text{Dy}^{3+}$ ,  $\text{Er}^{3+}$ ,  $\text{Sm}^{3+}$ ,  $\text{Gd}^{3+}$ ,  $\text{Ce}^{3+}$ ,  $\text{Pr}^{3+}$  and  $\text{Nd}^{3+}$ ). Adapted with permissions from [95]. Copyright Elsevier, 2012.

In addition to  $\text{Eu}^{2+}$  ions,  $\text{Cr}^{3+}$  ions have also been employed as dopants in  $\text{BaAl}_2\text{O}_4$ . Singh et al. prepared red-emitting  $\text{BaAl}_2\text{O}_4:\text{Cr}^{3+}$  phosphors via the urea combustion method [89]. The excitation spectra of this synthesized phosphor featured two broad bands with high intensities at 421 and 552 nm, which were ascribed to the  $\text{Cr}^{3+}$  ions in octahedral symmetry. The emission peak observed at 750 nm corresponded to the transition from  $\text{Cr}^{3+}$  ions. Vrankic et al. investigated the oxidation state of Cr dopant in a Cr-doped  $\text{BaAl}_2\text{O}_4$  structure using XRD and synchrotron-based X-ray absorption spectroscopy (XAS) [90].

Two different oxidation states for chromium ions were found.  $\text{Cr}^{6+}$  was observed in a small amount in an impure phase ( $\text{BaCrO}_4$ ), whereas  $\text{Cr}^{3+}$  was noted to participate in the formation of the doped  $\text{BaAl}_2\text{O}_4:\text{Cr}^{3+}$  phase, in which it behaved as a defect.

#### 4.3. Codoping of Barium Aluminate Phosphors with Various Trivalent Lanthanide Ions

The persistent luminescence of lanthanide-doped  $\text{BaAl}_2\text{O}_4$  phosphors can also be enhanced by codoping with trivalent lanthanide ions, similar to that in the other alkaline earth aluminates. Among the various lanthanide elements that have been used as codopants,  $\text{Eu}^{2+}$  and  $\text{Dy}^{3+}$  have been particularly successful as codopants in the synthesis of polycrystalline barium aluminate phosphors ( $\text{BaAl}_2\text{O}_4:\text{Eu}^{2+},\text{Dy}^{3+}$ ) [36,87,93,99]. The photoluminescence efficiency of the  $\text{Eu}^{2+}$ -doped  $\text{BaAl}_2\text{O}_4$  phosphor was observed to increase after codoping with  $\text{Dy}^{3+}$ ; this phosphor exhibited afterglow properties with the longest duration among the various  $\text{MAl}_2\text{O}_4:\text{Eu}^{2+},\text{Dy}^{3+}$  phosphors ( $\text{M} = \text{Sr}, \text{Ca}, \text{Ba}$ ).

Liu et al. reported that the codoping of  $\text{BaAl}_2\text{O}_4:\text{Eu}^{2+}$  with  $\text{Dy}^{3+}$  did not modify the positions of either the emission band or the excitation band; however the luminescence intensity and afterglow duration of the phosphor increased [36]. The generally accepted mechanism for the photoluminescence of  $\text{BaAl}_2\text{O}_4:\text{Eu}^{2+},\text{Dy}^{3+}$  is similar to that of  $\text{SrAl}_2\text{O}_4:\text{Eu}^{2+},\text{Dy}^{3+}$  and includes the following steps: (1) electron migration induced by UV radiation from the  $4f^65d^1$  levels in  $\text{Eu}^{2+}$  to the conduction band, (2) electron trapping from the conduction band to defects such as oxygen vacancies or codopant ions, (3) reverse electron migration from traps to the  $4f^65d^1$  levels in  $\text{Eu}^{2+}$ , and (4) radiative relaxation of the returned electron to the ground state of the luminescent center,  $\text{Eu}^{2+}$ . In this process, the type of codopant can affect the formation of electron traps, and therefore, the  $\text{Dy}^{3+}$  trap levels are presumed to be responsible for the long afterglow phosphorescence [36,93]. The effect of  $\text{Dy}^{3+}$  concentration on the afterglow of  $\text{BaAl}_2\text{O}_4:\text{Eu}^{2+},\text{Dy}^{3+}$  has also been investigated [87,99]. Stefani et al. found that the concentrations of both  $\text{Eu}^{2+}$  and  $\text{Dy}^{3+}$  play an important role in the determination of the crystallinity and luminescence properties of  $\text{BaAl}_2\text{O}_4:\text{Eu}^{2+},\text{Dy}^{3+}$  phosphors [87]. Rodrigues et al. investigated the concentration of  $\text{Eu}^{2+}/\text{Dy}^{3+}$  (in mol.% with respect to the amount of Ba) from 0.1/0.1 to 1.0/3.0, and found that the luminescence intensity increased as the  $\text{Eu}^{2+}$  and  $\text{Dy}^{3+}$  concentrations increased [99]. The high concentration of  $\text{Eu}^{2+}$  and the resulting enhancement of luminescence can be explained by an increase in the number of emitting centers. Increased  $\text{Dy}^{3+}$  concentration is also presumed to reduce the distance between the electron traps and the emitting center, which increases the efficiency of energy transfer.

$\text{Cr}^{3+}$  ions have also been employed as codopants in  $\text{BaAl}_2\text{O}_4:\text{Eu}^{2+}$ . Ryu et al. synthesized  $\text{BaAl}_2\text{O}_4:\text{Eu}^{2+},\text{Cr}^{3+}$  using various concentrations of  $\text{Cr}^{3+}$  [94]. Crystalline fibers were obtained via the different concentrations of  $\text{Cr}^{3+}$  (0.01, 0.05, and 0.1 mol%); fibers with larger dimensions were obtained at higher concentrations of doped Cr.

$\text{Ho}^{3+}$  ions have also been codoped in  $\text{BaAl}_2\text{O}_4:\text{Eu}^{2+}$  to facilitate the enhancement of photoluminescence. Liu et al. reported that the  $\text{BaAl}_2\text{O}_4:\text{Eu}^{2+},\text{Ho}^{3+}$  samples exhibited excitation and emission spectra with shapes and positions similar to those from  $\text{BaAl}_2\text{O}_4:\text{Eu}^{2+},\text{Dy}^{3+}$  but with slightly lower emission intensities [101].

Annah et al. systematically investigated the use of several trivalent rare-earth ions ( $\text{Dy}^{3+}, \text{Nd}^{3+}, \text{Gd}^{3+}, \text{Sm}^{3+}, \text{Ce}^{3+}, \text{Er}^{3+}, \text{Pr}^{3+}$ , and  $\text{Tb}^{3+}$ ) as codopants in  $\text{BaAl}_2\text{O}_4:\text{Eu}^{2+}$  [95]. All tested samples were found to exhibit blue–green emission at  $\sim 500\text{nm}$ , which corresponds to the  $4f^6d^1-4f^7$  transitions of  $\text{Eu}^{2+}$ ; no changes were observed in the phase structure after codoping. The emission intensity of the  $\text{Er}^{3+}$ -codoped phosphor was noted to be the highest, and the afterglow of the  $\text{Nd}^{3+}$ -codoped phosphor was observed to be the longest.

## 5. Outlook

Lanthanide-activated alkaline earth aluminates phosphors are excellent luminescent materials and can have extensive applications. In this review, lanthanide-doped strontium aluminate-, calcium aluminate-, and barium-aluminate-based phosphors, which are among the popular alkaline earth aluminates, were discussed with an emphasis on their synthe-

sis methods, phosphorescence mechanisms, and the effects of dopants and codopants on phosphor properties. This systematic review featuring the development of various lanthanide-activated alkaline earth aluminate phosphors is expected to stimulate further research on lanthanide-based phosphors for applications in a wide range of areas. Various attempts have been made to optimize the synthesis methods and compositions of lanthanide-activated alkaline earth aluminates phosphors to improve their long-persistent luminescence properties; however, recent strategies involving nanomaterial engineering, which have been successfully implemented for different types of nanoparticles, can also be adopted to further enhance the luminescence properties of phosphors (Figure 5).

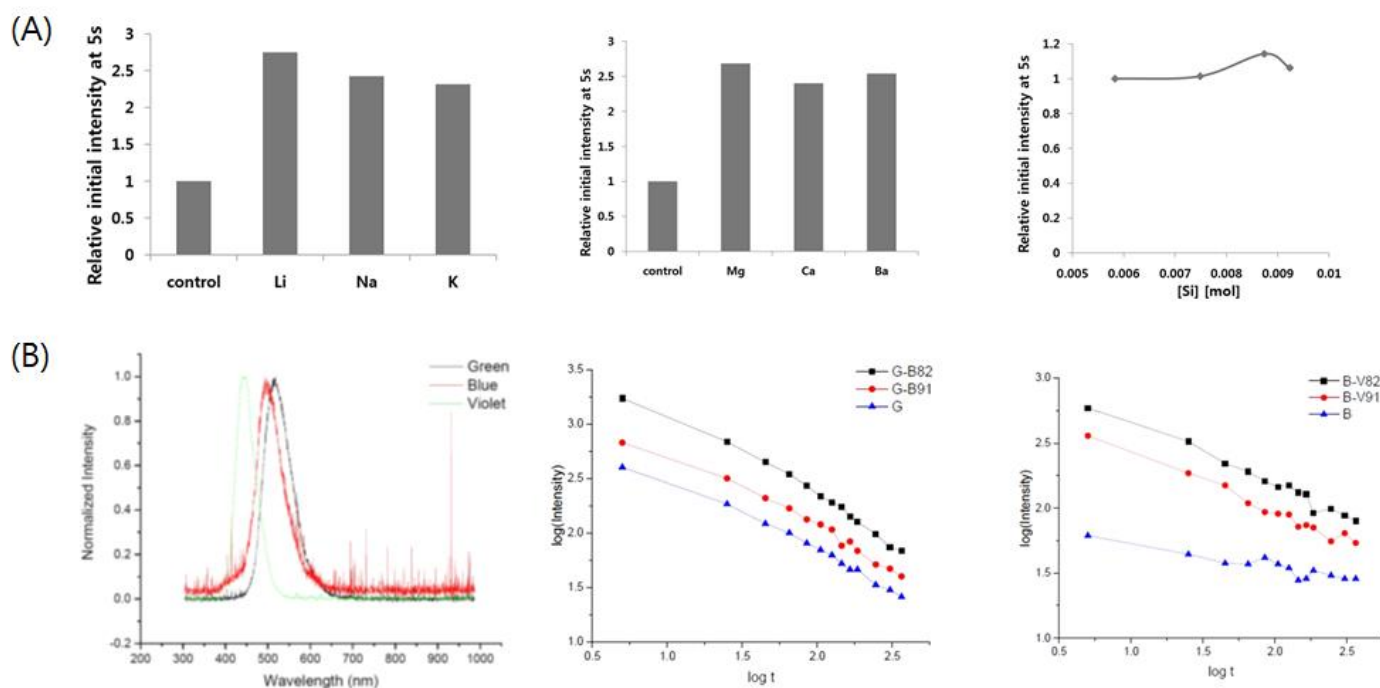


**Figure 5.** Various efforts to enhance the photoluminescence intensity of lanthanide-doped alkaline earth aluminate phosphors (A) Enhanced photoluminescence intensity by alkali metal (left), alkaline earth metal (middle), and Si (right) ions doping. Adapted from [12] under Creative Commons Attribution (CC BY) license. (B) (left) Emission spectra of the green ( $\text{SrAl}_2\text{O}_4:\text{Eu}^{2+},\text{Dy}^{3+}$ ), blue ( $\text{Sr}_4\text{Al}_{14}\text{O}_{25}:\text{Eu}^{2+},\text{Dy}^{3+}$ ), and violet ( $\text{CaAl}_2\text{O}_4:\text{Eu}^{2+},\text{Nd}^{3+}$ ) phosphors used for the phosphor mixing method with the aim of energy transfer between them. (middle) Photoluminescence decay curves in log scale for the green and blue phosphors mixed sample, showing enhanced luminescence intensity of green phosphor by mixing with the blue phosphor. (right) Photoluminescence decay curves in log scale for the blue and violet phosphors mixed sample, showing enhanced luminescence intensity of blue phosphor by mixing with the violet phosphor. Adapted from [14] under Creative Commons Attribution (CC BY) license.

Energy transfer between the different lanthanide ions in dual-emitting lanthanide-ion-codoped phosphors has been utilized to facilitate ratiometric temperature sensing and enhancement of photoluminescence of the phosphors. Energy transfer between two lanthanide codoped ions has been observed in several dual-color emitting phosphors, such as  $\text{Ba}_2\text{Y}(\text{BO}_3)_2\text{Cl}:\text{Bi}^{3+},\text{Eu}^{3+}$ ,  $\text{BaLu}_6(\text{Si}_2\text{O}_7)_2(\text{Si}_3\text{O}_{10}):\text{Ce}^{3+},\text{Tb}^{3+}$ , and  $\text{LaOBr}:\text{Ce}^{3+},\text{Tb}^{3+}$  [47,102]. Two emission peaks were observed herein because of the presence of two luminescence centers in these dual-emitting phosphors; their ratio was found to change with the extent of energy transfer. Applying this phenomenon, Zhang et al. demonstrated the ratiometric temperature sensing of  $\text{LaOBr}:\text{Ce}^{3+},\text{Tb}^{3+}$  over a wide temperature-sensing range (293–443 K) with a sensitivity of  $0.42\% \text{ K}^{-1}$  [103]. This approach has also been recently demonstrated in lanthanide-codoped aluminate phosphors with various colors, such as  $\text{SrAl}_2\text{O}_4:\text{Eu}^{2+},\text{Dy}^{3+}$ ,  $\text{Sr}_4\text{Al}_{14}\text{O}_{25}:\text{Eu}^{2+},\text{Dy}^{3+}$ , and  $\text{CaAl}_2\text{O}_4:\text{Eu}^{2+},\text{Nd}^{3+}$  as green, blue, and violet phosphors, respectively [14]. Novel protocols have been developed based on the effect of energy transfer

between spectrally different phosphors, and they were noted to significantly improve the afterglow intensities and lifetimes of green and blue phosphors. Multistep energy transfer between the three phosphors with different colors was also achieved, and a much higher afterglow intensity was generated:  $\sim 2$  times that via single-step energy transfer. Therefore, it is vital to consider the synthesis of various lanthanide-doped alkaline earth aluminate phosphors as a new strategy for the development of bright and long-persistent phosphors.

Distortion of crystal fields has also been induced via the introduction of impurities to facilitate the tuning of the luminescence properties of phosphor crystals [104]. Various alkali metals have been employed as dopants to increase the afterglow intensity and lifetime. Dhananjaya et al. observed that the photoluminescence intensity of the  $\text{Gd}_2\text{O}_3:\text{Eu}^{3+}$  phosphor remarkably increased after the incorporation of  $\text{Li}^+$ ,  $\text{Na}^+$ , and  $\text{K}^+$  into this phosphor [105]. Kim et al. also reported that the doping of  $\text{SrAl}_2\text{O}_4:\text{Eu}^{2+}, \text{Dy}^{3+}$ , and  $\text{CaAl}_2\text{O}_4:\text{Eu}^{2+}, \text{Nd}^{3+}$  phosphor with alkali metals ( $\text{Li}^+$ ,  $\text{Na}^+$ ,  $\text{K}^+$ ) and alkaline earth metals ( $\text{Mg}^{2+}$ ,  $\text{Ca}^{2+}$ ,  $\text{Ba}^{2+}$ ) can significantly boost the phosphorescence intensity and increase the afterglow lifetime [12,81]. These apparently imply that  $\text{Si}^{4+}$  doping is also effective for enhancing the phosphorescence intensity. Upon the incorporation of  $\text{Si}^{4+}$  into the  $\text{SrAl}_2\text{O}_4$  crystal, the local symmetry of the crystal structure was presumed to be broken owing to the smaller size of  $\text{Si}^{4+}$  ( $\sim 40$  pm) compared to that of  $\text{Al}^{3+}$  (53 pm). Therefore, an increase in luminescence was observed for both phosphors at the optimal concentration of  $\text{Si}^{4+}$ . The effect of incorporation of additional impurities on photoluminescence is presumed to be a result of the local distortion of the crystal field surrounding the luminescence center, which is known to considerably affect the  $f-d$  transitions. Such impurity effects are expected to play an important role in the future development of effective codopants.

Ideas for the straightforward fabrication of nanoparticles with desirable shapes and sizes have also been suggested. Liu et al. attempted to control the size, shape, and surface properties of rare-earth-doped nanomaterials at the atomic scale using oleate anions ( $\text{OA}^-$ ) and molecules (OAH) [106]. This level of control was observed to facilitate the fabrication of various sub-50 nm-sized monodispersed nanoparticles. Similarly, Sui et al. reported the use of oleate salts as ligands that can shorten the reaction time (down to 5 min) during the synthesis of the ultrasmall ( $\sim 13$  nm) hexagonal phase of the  $\text{NaYF}_3$  nanocrystals; this was facilitated via induction of the orderly arrangement of  $\text{Y}^{3+}$  and lowering of the energy barrier for the phase transition to occur [107].

Overall, recent approaches based on nanomaterial engineering can be expected to be readily expanded to lanthanide-doped alkaline earth aluminate phosphor systems for the enhancement of their photoluminescence properties. However, results from previous studies on the design of phosphors for obtaining desirable sizes of the phosphor particles need to be carefully considered. Most of the studies discussed in this review involve bulk structures; however, the properties of nanoparticles, such as luminescence and physical and chemical properties, can be different at the nanoscale. The coordination complex of a doped lanthanide ion can be easily distorted in nanoparticles compared to that in the bulk lattice because nanophosphors typically have large surface areas and high densities of interfacial boundaries. Recent approaches based on theoretical modeling are expected to play an essential role in the estimation of the photoluminescence characteristics and mechanisms in newly designed nanophosphors. The development of new lanthanide-doped phosphors should include systematic characterization to investigate the sizes and scales involved.

## 6. Conclusions

Considerable attempts have been made to develop bright and long-persistent lanthanide-doped alkaline earth aluminate phosphors for replacing the conventionally and extensively used ZnS phosphors; as a result, the luminescence properties of such phosphors have been significantly improved. Various synthesis methods have been employed to prepare lanthanide-doped alkaline earth aluminate phosphors, and their pros and cons have been found to arise from the different reaction temperatures, reaction phases (solid or liquid), and particle size of the product. The luminescence properties of these aluminate

phosphors are mainly determined by the compositions of the doped lanthanide ions and the host matrix. The localized environment surrounding the lanthanide activator, which is a luminescence center, appears to play a crucial role in persistent luminescence. It is important to determine the effect of the synthesis steps and compositions of phosphors on the persistent luminescence because subtle changes in the phosphor synthesis conditions can lead to significant variations in their luminescence properties. The development of lanthanide-doped alkaline earth aluminate phosphors has great potential; such phosphors can also be expected to find application in a wide range of areas.

**Funding:** Hanyang University (HY-2018).

**Acknowledgments:** This work was supported by the research fund of Hanyang University (HY-2018)

**Conflicts of Interest:** The authors declare no conflict of interest.

## References

1. Brahme, A. *Comprehensive Biomedical Physics*; Elsevier: Amsterdam, The Netherlands, 2014.
2. Ray, B. Phosphors and Luminescence. In *Electronic Materials*; Springer: Berlin/Heidelberg, Germany, 1991; pp. 211–223.
3. Lehmann, W. Activators and co-activators in calcium sulfide phosphors. *J. Lumin.* **1972**, *5*, 87–107. [[CrossRef](#)]
4. Potyrailo, R.A.; Maier, W.F. *Combinatorial and High-Throughput Discovery and Optimization of Catalysts and Materials*; CRC Press: Boca Raton, FL, USA, 2006.
5. Matsuzawa, T.; Aoki, Y.; Takeuchi, N.; Murayama, Y. A new long phosphorescent phosphor with high brightness, SrAl<sub>2</sub>O<sub>4</sub>: Eu<sup>2+</sup>, Dy<sup>3+</sup>. *J. Electrochem. Soc.* **1996**, *143*, 2670. [[CrossRef](#)]
6. Zúñiga-Rivera, N.; Salas-Castillo, P.; Chernov, V.; Díaz-Torres, L.; Meléndrez, R.; García-Gutierrez, R.; Carrillo-Torres, R.; Barboza-Flores, M. Thermally and optically stimulated luminescence in long persistent orthorhombic strontium aluminates doped with Eu, Dy and Eu, Nd. *Opt. Mater.* **2017**, *67*, 91–97. [[CrossRef](#)]
7. Nazarov, M.; Brik, M.G.; Spassky, D.; Tsukerblat, B. Crystal field splitting of 5d states and luminescence mechanism in SrAl<sub>2</sub>O<sub>4</sub>: Eu<sup>2+</sup> phosphor. *J. Lumin.* **2017**, *182*, 79–86. [[CrossRef](#)]
8. Peng, M.; Hong, G. Reduction from Eu<sup>3+</sup> to Eu<sup>2+</sup> in BaAl<sub>2</sub>O<sub>4</sub>: Eu phosphor prepared in an oxidizing atmosphere and luminescent properties of BaAl<sub>2</sub>O<sub>4</sub>: Eu. *J. Lumin.* **2007**, *127*, 735–740. [[CrossRef](#)]
9. Freeda, M.; Subash, T. Preparation and Characterization of Praseodymium doped Calcium Aluminate nanophosphor (CaAl<sub>2</sub>O<sub>4</sub>: Pr) by sol-gel method. *Mater. Today Proc.* **2017**, *4*, 4266–4273. [[CrossRef](#)]
10. Blasse, G.; Wanamaker, W. Fluorescence of Eu<sup>2+</sup> activated silicates. *Philips Res. Rep.* **1968**, *23*, 189.
11. Anesh, M.; Gulrez, S.K.; Anis, A.; Shaikh, H.; Ali Mohsin, M.; Al-Zahrani, S. Developments in Eu<sup>2+</sup>-Doped Strontium Aluminate and Polymer/Strontium Aluminate Composite. *Adv. Polym. Technol.* **2014**, *33*. [[CrossRef](#)]
12. Kim, D.; Kim, H.-E.; Kim, C.-H. Effect of composition and impurities on the phosphorescence of green-emitting alkaline earth aluminate phosphor. *PLoS ONE* **2016**, *11*, e0145434. [[CrossRef](#)]
13. Saines, P.J.; Elcombe, M.M.; Kennedy, B.J. Lanthanide distribution in some doped alkaline earth aluminates and gallates. *J. Solid State Chem.* **2006**, *179*, 613–622. [[CrossRef](#)]
14. Kim, D.; Kim, H.-E.; Kim, C.-H. Enhancement of Long-Persistent Phosphorescence by Solid-State Reaction and Mixing of Spectrally Different Phosphors. *ACS Omega* **2020**. [[CrossRef](#)] [[PubMed](#)]
15. Shang, M.; Wang, J.; Dang, P.; Lian, H.; Lin, J. Two-Step Sol-Gel Synthetic Strategy for Highly Dispersed Eu<sup>2+</sup> Luminescence Centers for Tuning Emission. *Adv. Photonics Res.* **2020**, *1*, 2000028. [[CrossRef](#)]
16. Fritzen, D.L.; Giordano, L.; Rodrigues, L.C.; Monteiro, J.H. Opportunities for Persistent Luminescent Nanoparticles in Luminescence Imaging of Biological Systems and Photodynamic Therapy. *Nanomaterials* **2020**, *10*, 2015. [[CrossRef](#)]
17. Francis, B.; Nolasco, M.M.; Brandão, P.; Ferreira, R.A.; Carvalho, R.S.; Cremona, M.; Carlos, L.D. Efficient Visible-Light-Excitable Eu<sup>3+</sup> Complexes for Red Organic Light-Emitting Diodes. *Eur. J. Inorg. Chem.* **2020**. [[CrossRef](#)]
18. Tiwari, A.; Dhoble, S. Tunable lanthanide/transition metal ion-doped novel phosphors for possible application in w-LEDs: A review. *Luminescence* **2020**, *35*, 4–33. [[CrossRef](#)] [[PubMed](#)]
19. Nimbalkar, M.; Yawalkar, M.; Mahajan, N.; Dhoble, S. Potential of Luminescent Materials In Phototherapy. *Photodiagnosis Photodyn. Ther.* **2020**, 102082. [[CrossRef](#)]
20. Kohale, R.; Dhoble, S. Development of Dy<sup>3+</sup> activated K<sub>2</sub>MgP<sub>2</sub>O<sub>7</sub> pyrophosphate phosphor for energy saving lamp. *J. Lumin.* **2013**, *138*, 153–156. [[CrossRef](#)]
21. Huy, B.T.; Gerelkhuu, Z.; Chung, J.W.; Dao, V.-D.; Ajithkumar, G.; Lee, Y.-I. Enhanced light harvesting with chromium in NaLu<sub>0.70-x</sub>Gd<sub>0.10</sub>F<sub>4</sub>:Yb<sub>0.18</sub>Er<sub>0.02</sub>Cr<sub>x</sub> (0 ≤ x ≤ 0.25) upconversion system. *Mater. Sci. Eng. B* **2017**, *223*, 91–97. [[CrossRef](#)]
22. Markose, K.K.; Anjana, R.; Antony, A.; Jayaraj, M. Synthesis of Yb<sup>3+</sup>/Er<sup>3+</sup> co-doped Y<sub>2</sub>O<sub>3</sub>, YOF and YF<sub>3</sub> UC phosphors and their application in solar cell for sub-bandgap photon harvesting. *J. Lumin.* **2018**, *204*, 448–456. [[CrossRef](#)]
23. Qin, X.; Liu, X.; Huang, W.; Bettinelli, M.; Liu, X. Lanthanide-activated phosphors based on 4f-5d optical transitions: Theoretical and experimental aspects. *Chem. Rev.* **2017**, *117*, 4488–4527. [[CrossRef](#)] [[PubMed](#)]

24. Joos, J.J.; Smet, P.F.; Seijo, L.; Barandiarán, Z. Insights into the complexity of the excited states of Eu-doped luminescent materials. *Inorg. Chem. Front.* **2020**, *7*, 871–888. [\[CrossRef\]](#)
25. Marin, R.; Jaque, D. Doping Lanthanide Ions in Colloidal Semiconductor Nanocrystals for Brighter Photoluminescence. *Chem. Rev.* **2021**, *121*, 1425–1462. [\[CrossRef\]](#)
26. Dorenbos, P. Energy of the first  $4f7 \rightarrow 4f65d$  transition of  $\text{Eu}^{2+}$  in inorganic compounds. *J. Lumin.* **2003**, *104*, 239–260. [\[CrossRef\]](#)
27. Sahu, I.P.; Bisen, D.; Brahme, N.; Tamrakar, R.K.; Shrivastava, R. Luminescence studies of dysprosium doped strontium aluminate white light emitting phosphor by combustion route. *J. Mater. Sci. Mater. Electron.* **2015**, *26*, 8824–8839. [\[CrossRef\]](#)
28. Nazarov, M.; Brik, M.; Spassky, D.; Tsukerblat, B.; Nazida, A.N.; Ahmad-Fauzi, M. Structural and electronic properties of  $\text{SrAl}_2\text{O}_4:\text{Eu}^{2+}$  from density functional theory calculations. *J. Alloys Compd.* **2013**, *573*, 6–10. [\[CrossRef\]](#)
29. Lindop, A.; Matthews, C.; Goodwin, D. The refined structure of  $\text{SrO} \cdot 6\text{Al}_2\text{O}_3$ . *Acta Crystallogr. Sect. B Struct. Crystallogr. Cryst. Chem.* **1975**, *31*, 2940–2941. [\[CrossRef\]](#)
30. Gedekar, K.; Wankhede, S.; Moharil, S.; Belekar, R. d–f luminescence of  $\text{Ce}^{3+}$  and  $\text{Eu}^{2+}$  ions in  $\text{BaAl}_2\text{O}_4$ ,  $\text{SrAl}_2\text{O}_4$  and  $\text{CaAl}_2\text{O}_4$  phosphors. *J. Adv. Ceram.* **2017**, *6*, 341–350. [\[CrossRef\]](#)
31. Kim, S.J.; Won, H.I.; Hayk, N.; Won, C.W.; Jeon, D.Y.; Kirakosyan, A.G. Preparation and characterization of  $\text{Sr}_4\text{Al}_2\text{O}_7:\text{Eu}^{3+}, \text{Eu}^{2+}$  phosphors. *Mater. Sci. Eng. B* **2011**, *176*, 1521–1525. [\[CrossRef\]](#)
32. Fu, Z.; Ma, L.; Sahi, S.; Hall, R.; Chen, W. Influence of doping concentration on valence states of europium in  $\text{SrAl}_2\text{O}_4$ : Eu phosphors. *J. Lumin.* **2013**, *143*, 657–662. [\[CrossRef\]](#)
33. Mindru, I.; Gingasu, D.; Patron, L.; Marinescu, G.; Calderon-Moreno, J.M.; Diamandescu, L.; Secu, M.; Oprea, O.  $\text{Tb}^{3+}$ -doped alkaline-earth aluminates: Synthesis, characterization and optical properties. *Mater. Res. Bull.* **2017**, *85*, 240–248. [\[CrossRef\]](#)
34. Katsumata, T.; Nabae, T.; Sasajima, K.; Matsuzawa, T. Growth and characteristics of long persistent  $\text{SrAl}_2\text{O}_4$ - and  $\text{CaAl}_2\text{O}_4$ -based phosphor crystals by a floating zone technique. *J. Cryst. Growth* **1998**, *183*, 361–365. [\[CrossRef\]](#)
35. Jia, W.; Yuan, H.; Lu, L.; Liu, H.; Yen, W.M. Crystal growth and characterization of  $\text{Eu}^{2+}, \text{Dy}^{3+}:\text{SrAl}_2\text{O}_4$  and  $\text{Eu}^{2+}, \text{Nd}^{3+}:\text{CaAl}_2\text{O}_4$  by the LHPG method. *J. Cryst. Growth* **1999**, *200*, 179–184. [\[CrossRef\]](#)
36. Lin, Y.; Zhang, Z.; Tang, Z.; Zhang, J.; Zheng, Z.; Lu, X. The characterization and mechanism of long afterglow in alkaline earth aluminates phosphors co-doped by  $\text{Eu}_2\text{O}_3$  and  $\text{Dy}_2\text{O}_3$ . *Mater. Chem. Phys.* **2001**, *70*, 156–159. [\[CrossRef\]](#)
37. Lu, Y.; Li, Y.; Xiong, Y.; Wang, D.; Yin, Q.  $\text{SrAl}_2\text{O}_4:\text{Eu}^{2+}, \text{Dy}^{3+}$  phosphors derived from a new sol–gel route. *Microelectron. J.* **2004**, *35*, 379–382. [\[CrossRef\]](#)
38. Qiu, Z.; Zhou, Y.; Lü, M.; Zhang, A.; Ma, Q. Combustion synthesis of long-persistent luminescent  $\text{MAl}_2\text{O}_4:\text{Eu}^{2+}, \text{R}^{3+}$  (M = Sr, Ba, Ca, R = Dy, Nd and La) nanoparticles and luminescence mechanism research. *Acta Mater.* **2007**, *55*, 2615–2620. [\[CrossRef\]](#)
39. Mothudi, B.M.; Ntwaeaborwa, O.; Botha, J.; Swart, H. Photoluminescence and phosphorescence properties of  $\text{MAl}_2\text{O}_4:\text{Eu}^{2+}, \text{Dy}^{3+}$  (M = Ca, Ba, Sr) phosphors prepared at an initiating combustion temperature of 500 °C. *Phys. B Condens. Matter* **2009**, *404*, 4440–4444. [\[CrossRef\]](#)
40. Aroz, R.; Lennikov, V.; Cases, R.; Sanjuán, M.L.; Germán, F.; Muñoz, E. Laser synthesis and luminescence properties of  $\text{SrAl}_2\text{O}_4:\text{Eu}^{2+}, \text{Dy}^{3+}$  phosphors. *J. Eur. Ceram. Soc.* **2012**, *32*, 4363–4369. [\[CrossRef\]](#)
41. Gültekin, S.; Yıldırım, S.; Yılmaz, O.; Keskin, İ.Ç.; Katı, M.İ.; Çelik, E. Structural and optical properties of  $\text{SrAl}_2\text{O}_4:\text{Eu}^{2+}/\text{Dy}^{3+}$  phosphors synthesized by flame spray pyrolysis technique. *J. Lumin.* **2019**, *206*, 59–69. [\[CrossRef\]](#)
42. Halefoglu, Y.; Yüksel, M.; Derin, H.; Can, N.; Topaksu, M.; Ozturk, E.; Karacaoğlu, E. Preparation and photoluminescence properties of aluminate phosphors produced by combustion synthesis. *Appl. Radiat. Isot.* **2018**, *142*, 46–50. [\[CrossRef\]](#)
43. Aitasalo, T.; Dereñ, P.; Hölsä, J.; Jungner, H.; Krupa, J.-C.; Lastusaari, M.; Legendziewicz, J.; Niittykoski, J.; Strek, W. Persistent luminescence phenomena in materials doped with rare earth ions. *J. Solid State Chem.* **2003**, *171*, 114–122. [\[CrossRef\]](#)
44. Chernov, V.; Salas-Castillo, P.; Díaz-Torres, L.; Zúñiga-Rivera, N.; Ruiz-Torres, R.; Meléndrez, R.; Barboza-Flores, M. Thermoluminescence and infrared stimulated luminescence in long persistent monoclinic  $\text{SrAl}_2\text{O}_4:\text{Eu}^{2+}, \text{Dy}^{3+}$  and  $\text{SrAl}_2\text{O}_4:\text{Eu}^{2+}, \text{Nd}^{3+}$  phosphors. *Opt. Mater.* **2019**, *92*, 46–52. [\[CrossRef\]](#)
45. Song, H.; Chen, D. Combustion synthesis and luminescence properties of  $\text{SrAl}_2\text{O}_4:\text{Eu}^{2+}, \text{Dy}^{3+}, \text{Tb}^{3+}$  phosphor. *Lumin. J. Biol. Chem. Lumin.* **2007**, *22*, 554–558. [\[CrossRef\]](#)
46. Hölsä, J.; Jungner, H.; Lastusaari, M.; Niittykoski, J. Persistent luminescence of  $\text{Eu}^{2+}$  doped alkaline earth aluminates,  $\text{MAl}_2\text{O}_4:\text{Eu}^{2+}$ . *J. Alloys Compd.* **2001**, *323*, 326–330. [\[CrossRef\]](#)
47. Li, K.; Lian, H.; Han, Y.; Shang, M.; Van Deun, R.; Lin, J.  $\text{BaLu}_6(\text{Si}_2\text{O}_7)_2(\text{Si}_3\text{O}_{10})$ :  $\text{Ce}^{3+}, \text{Tb}^{3+}$ : A novel blue-green emission phosphor via energy transfer for UV LEDs. *Dye. Pigment.* **2017**, *139*, 701–707. [\[CrossRef\]](#)
48. He, Q.; Fu, R.; Zhu, H.; He, H.; Song, X.; Liu, X. Synthesis and luminescence enhancement of  $\text{Ca}_y\text{Sr}_{4-x-y}\text{Al}_2\text{O}_7:x\text{Eu}^{2+}$  phosphors by a novel halide-assisted solid-state reaction method. *J. Mater. Sci. Mater. Electron.* **2018**, *29*, 10487–10493. [\[CrossRef\]](#)
49. Singh, V.; Rao, T.G.; Zhu, J.-J. Preparation, luminescence and defect studies of  $\text{Eu}^{2+}$ -activated strontium hexa-aluminate phosphor prepared via combustion method. *J. Solid State Chem.* **2006**, *179*, 2589–2594. [\[CrossRef\]](#)
50. Havasi, V.; Tátrai, D.; Szabó, G.; Varga, E.; Erdőhelyi, A.; Sipos, G.; Kónya, Z.; Kukovecz, Á. On the effects of milling and thermal regeneration on the luminescence properties of  $\text{Eu}^{2+}$  and  $\text{Dy}^{3+}$  doped strontium aluminate phosphors. *J. Lumin.* **2020**, *219*, 116917. [\[CrossRef\]](#)
51. Zhang, B.; Liu, Q.; Yan, W.; Chen, Y.; Shen, A.; Zhang, H. Relation between structure conversion and spectra-tuning properties of  $\text{Eu}^{2+}$ -doped strontium aluminate phosphor. *J. Mater. Sci.* **2017**, *52*, 8188–8199. [\[CrossRef\]](#)

52. Misevicius, M.; Scit, O.; Grigoraviciute-Puroniene, I.; Degutis, G.; Bogdanoviciene, I.; Kareiva, A. Sol-gel synthesis and investigation of un-doped and Ce-doped strontium aluminates. *Ceram. Int.* **2012**, *38*, 5915–5924. [[CrossRef](#)]
53. Dutczak, D.; Jüstel, T.; Ronda, C.; Meijerink, A.  $\text{Eu}^{2+}$  luminescence in strontium aluminates. *Phys. Chem. Chem. Phys.* **2015**, *17*, 15236–15249. [[CrossRef](#)]
54. Clabau, F.; Rocquefelte, X.; Jobic, S.; Deniard, P.; Whangbo, M.-H.; Garcia, A.; Le Mercier, T. Mechanism of phosphorescence appropriate for the long-lasting phosphors  $\text{Eu}^{2+}$ -doped  $\text{SrAl}_2\text{O}_4$  with codopants  $\text{Dy}^{3+}$  and  $\text{B}^{3+}$ . *Chem. Mater.* **2005**, *17*, 3904–3912. [[CrossRef](#)]
55. Bierwagen, J.; Delgado, T.; Jiranek, G.; Yoon, S.; Gartmann, N.; Walfort, B.; Pollnau, M.; Hagemann, H. Probing traps in the persistent phosphor  $\text{SrAl}_2\text{O}_4$ :  $\text{Eu}^{2+}$ ,  $\text{Dy}^{3+}$ ,  $\text{B}^{3+}$ -A wavelength, temperature and sample dependent thermoluminescence investigation. *J. Lumin.* **2020**, *222*, 117113. [[CrossRef](#)]
56. Vitola, V.; Millers, D.; Bite, I.; Smits, K.; Spustaka, A. Recent progress in understanding the persistent luminescence in  $\text{SrAl}_2\text{O}_4$ :  $\text{Eu}$ ,  $\text{Dy}$ . *Mater. Sci. Technol.* **2019**, *35*, 1661–1677. [[CrossRef](#)]
57. Li, G.; Tian, Y.; Zhao, Y.; Lin, J. Recent progress in luminescence tuning of  $\text{Ce}^{3+}$  and  $\text{Eu}^{2+}$ -activated phosphors for pc-WLEDs. *Chem. Soc. Rev.* **2015**, *44*, 8688–8713. [[CrossRef](#)]
58. Menon, S.G.; Bedyal, A.; Pathak, T.; Kumar, V.; Swart, H.C.  $\text{Sr}_4\text{Al}_{14}\text{O}_{25}$ :  $\text{Eu}^{2+}$ ,  $\text{Dy}^{3+}$ @ $\text{ZnO}$  nanocomposites as highly efficient visible light photocatalysts for the degradation of aqueous methyl orange. *J. Alloys Compd.* **2020**, 158370. [[CrossRef](#)]
59. Chithambo, M. Thermal assistance in the optically stimulated luminescence of superluminous  $\text{Sr}_4\text{Al}_{14}\text{O}_{25}$ :  $\text{Eu}^{2+}$ ,  $\text{Dy}^{3+}$ . *Phys. B Condens. Matter* **2020**, 412722. [[CrossRef](#)]
60. Morrison, C.A. Host dependence of the rare-earth ion energy separation  $4f^N-4f^{N-1}nl$ . *J. Chem. Phys.* **1980**, *72*, 1001–1002. [[CrossRef](#)]
61. Mishra, S.; Mishra, A.; Luyt, A.; Revaprasadu, N.; Hillie, K.; vdM Steyn, W.; Coetsee, E.; Swart, H. Ethyl vinyl acetate copolymer— $\text{SrAl}_2\text{O}_4$ : $\text{Eu}$ , $\text{Dy}$  and  $\text{Sr}_4\text{Al}_{14}\text{O}_{25}$ : $\text{Eu}$ , $\text{Dy}$  phosphor-based composites: Preparation and material properties. *J. Appl. Polym. Sci.* **2010**, *115*, 579–587. [[CrossRef](#)]
62. Vitola, V.; Bite, I.; Millers, D.; Zolotarjovs, A.; Laganovska, K.; Smits, K.; Spustaka, A. The boron effect on low temperature luminescence of  $\text{SrAl}_2\text{O}_4$ :  $\text{Eu}$ ,  $\text{Dy}$ . *Ceram. Int.* **2020**, *46*, 26377–26381. [[CrossRef](#)]
63. Zhang, S.; Nakai, Y.; Tsuboi, T.; Huang, Y.; Seo, H.J. Luminescence and microstructural features of  $\text{Eu}$ -activated  $\text{LiBaPO}_4$  phosphor. *Chem. Mater.* **2011**, *23*, 1216–1224. [[CrossRef](#)]
64. Chen, Y.; Li, Y.; Wang, J.; Wu, M.; Wang, C. Color-tunable phosphor of  $\text{Eu}^{2+}$  and  $\text{Mn}^{2+}$  codoped  $\text{Ca}_2\text{Sr}(\text{PO}_4)_2$  for UV light-emitting diodes. *J. Phys. Chem. C* **2014**, *118*, 12494–12499. [[CrossRef](#)]
65. Kareiva, A. Aqueous sol-gel synthesis methods for the preparation of garnet crystal structure compounds. *Mater. Sci.* **2011**, *17*, 428–436. [[CrossRef](#)]
66. Suta, M.; Lavoie-Cardinal, F.; Wickleder, C. Underestimated color centers: Defects as useful reducing agents in lanthanide-activated luminescent materials. *Angew. Chem. Int. Ed.* **2020**, *59*, 10949–10954. [[CrossRef](#)] [[PubMed](#)]
67. Du, H.; Castaing, V.; Guo, D.; Viana, B. Rare-earths doped-nanoparticles prepared by pulsed laser ablation in liquids. *Ceram. Int.* **2020**, *46*, 26299–26308. [[CrossRef](#)]
68. Delgado, T.; Bierwagen, J.; Gartmann, N.; Walfort, B.; Kinski, I.; Pollnau, M.; Hagemann, H. Characterization and afterglow of  $\text{SrAl}_2\text{O}_4$ :  $\text{Eu}$ ,  $\text{Dy}$  for various phosphor applications. In Proceedings of the Fiber Lasers and Glass Photonics: Materials through Applications II, Online. 6–10 April 2020; p. 113571.
69. Homayoni, H.; Sahi, S.; Ma, L.; Zhang, J.; Mohapatra, J.; Liu, P.; Sotelo, A.P.; Macaluso, R.T.; Davis, T.; Chen, W. X-ray excited luminescence and persistent luminescence of  $\text{Sr}_2\text{MgSi}_2\text{O}_7$ :  $\text{Eu}^{2+}$ ,  $\text{Dy}^{3+}$  and their associations with synthesis conditions. *J. Lumin.* **2018**, *198*, 132–137. [[CrossRef](#)]
70. Zhao, L.; Mao, J.; Jiang, B.; Wei, X.; Yin, M.; Chen, Y. A new yellow long persistent luminescence phosphor  $\text{Ca}_2\text{Al}_2\text{SiO}_7$ :  $\text{Eu}^{2+}$ ,  $\text{Tm}^{3+}$  found by co-doping  $\text{Ln}^{3+}$  ( $\text{Ln} = \text{Ce}, \text{Pr}, \text{Nd}, \text{Sm}, \text{Gd}, \text{Tb}, \text{Dy}, \text{Ho}, \text{Er}, \text{Tm}, \text{Yb}, \text{Lu}$ ) with  $\text{Eu}^{2+}$  in  $\text{Ca}_2\text{Al}_2\text{SiO}_7$  host. *J. Lumin.* **2019**, *206*, 6–10. [[CrossRef](#)]
71. Hai, O.; Ren, Q.; Wu, X.; Zhang, Q.; Zhang, Z.; Zhang, Z. Insights into the element gradient in the grain and luminescence mechanism of the long afterglow material  $\text{Sr}_2\text{MgSi}_2\text{O}_7$ :  $\text{Eu}^{2+}$ ,  $\text{Dy}^{3+}$ . *J. Alloys Compd.* **2019**, *779*, 892–899. [[CrossRef](#)]
72. Dorenbos, P. Mechanism of persistent luminescence in  $\text{Eu}^{2+}$  and  $\text{Dy}^{3+}$  codoped aluminate and silicate compounds. *J. Electrochem. Soc.* **2005**, *152*, H107. [[CrossRef](#)]
73. Rezende, M.d.S.; Montes, P.J.; Soares, F.d.S.; Santos, C.d.; Valerio, M.E. Influence of co-dopant in the europium reduction in  $\text{SrAl}_2\text{O}_4$  host. *J. Synchrotron Radiat.* **2014**, *21*, 143–148. [[CrossRef](#)]
74. Aitasalo, T.; Hölsä, J.; Jungner, H.; Krupa, J.-C.; Lastusaari, M.; Legendziewicz, J.; Niittykoski, J. Effect of temperature on the luminescence processes of  $\text{SrAl}_2\text{O}_4$ :  $\text{Eu}^{2+}$ . *Radiat. Meas.* **2004**, *38*, 727–730. [[CrossRef](#)]
75. Aitasalo, T.; Hölsä, J.; Jungner, H.; Lastusaari, M.; Niittykoski, J. Mechanisms of persistent luminescence in  $\text{Eu}^{2+}$ ,  $\text{RE}^{3+}$  doped alkaline earth aluminates. *J. Lumin.* **2001**, *94*, 59–63. [[CrossRef](#)]
76. Swati, G.; Jaiswal, V.V.; Haranath, D. Rare-earth doping in afterglow oxide phosphors: Materials, persistence mechanisms, and dark vision display applications. In *Spectroscopy of Lanthanide Doped Oxide Materials*; Elsevier: Cambridge, UK, 2020; pp. 393–425.
77. Jeong, J.; Kim, J.H.; Shim, J.H.; Hwang, N.S.; Heo, C.Y. Bioactive calcium phosphate materials and applications in bone regeneration. *Biomater. Res.* **2019**, *23*, 1–11. [[CrossRef](#)]

78. Zeng, C.; Feng, W.-L.; Chen, Z. Effect of boric acid on structure, morphology and luminescent properties of divalent europium doped calcium aluminate phosphors. *Optik* **2014**, *125*, 1252–1254. [CrossRef]
79. Freeda, M.; Subash, T. Comparison of Photoluminescence studies of Lanthanum, Terbium doped Calcium Aluminate nanophosphors (CaAl<sub>2</sub>O<sub>4</sub>: La, CaAl<sub>2</sub>O<sub>4</sub>: Tb) by sol-gel method. *Mater. Today Proc.* **2017**, *4*, 4302–4307. [CrossRef]
80. Zhao, C.; Chen, D. Synthesis of CaAl<sub>2</sub>O<sub>4</sub>: Eu, Nd long persistent phosphor by combustion processes and its optical properties. *Mater. Lett.* **2007**, *61*, 3673–3675. [CrossRef]
81. Kim, D.; Kim, H.-E.; Kim, C.-H. Development of a blue emitting calcium-aluminate phosphor. *PLoS ONE* **2016**, *11*, e0162920. [CrossRef]
82. Lin, Y.; Tang, Z.; Zhang, Z.; Nan, C. Influence of co-doping different rare earth ions on the luminescence of CaAl<sub>2</sub>O<sub>4</sub>-based phosphors. *J. Eur. Ceram. Soc.* **2003**, *23*, 175–178. [CrossRef]
83. Dougill, M.W. Crystal structure of calcium monoaluminate. *Nature* **1957**, *180*, 292–293. [CrossRef]
84. Guo, C.; Luan, L.; Chen, C.; Huang, D.; Su, Q. Preparation of Y<sub>2</sub>O<sub>2</sub>S: Eu<sup>3+</sup> phosphors by a novel decomposition method. *Mater. Lett.* **2008**, *62*, 600–602. [CrossRef]
85. Madhukumar, K.; Rajendra Babu, K.; Ajith Prasad, K.; James, J.; Elias, T.; Padmanabhan, V.; Nair, C. Luminescence studies of rare earth doped calcium aluminate phosphors. *Int. J. Mod. Phys. B* **2007**, *21*, 1971–1980. [CrossRef]
86. Singh, V.; Natarajan, V.; Zhu, J.-J. Luminescence and EPR investigations of Mn activated calcium aluminate prepared via combustion method. *Opt. Mater.* **2007**, *30*, 468–472. [CrossRef]
87. Stefani, R.; Rodrigues, L.C.V.; Carvalho, C.A.A.d.; Felinto, M.C.F.d.C.; Brito, H.F.d.; Lastusaari, M.; Hölsä, J. Persistent luminescence of Eu<sup>2+</sup> and Dy<sup>3+</sup> doped barium aluminate (BaAl<sub>2</sub>O<sub>4</sub>: Eu<sup>2+</sup>, Dy<sup>3+</sup>) materials. *Opt. Mater.* **2009**, *31*, 1815–1818. [CrossRef]
88. Jia, D.; Wang, X.-j.; Van der Kolk, E.; Yen, W. Site dependent thermoluminescence of long persistent phosphorescence of BaAl<sub>2</sub>O<sub>4</sub>: Ce<sup>3+</sup>. *Opt. Commun.* **2002**, *204*, 247–251. [CrossRef]
89. Singh, V.; Chakradhar, R.; Rao, J.; Zhu, J.-J. Studies on red-emitting Cr<sup>3+</sup> doped barium aluminate phosphor obtained by combustion process. *Mater. Chem. Phys.* **2008**, *111*, 143–148. [CrossRef]
90. Vrankić, M.; Gržeta, B.; Lützenkirchen-Hecht, D.; Bosnar, S.; Šarić, A. Chromium environment within Cr-doped BaAl<sub>2</sub>O<sub>4</sub>: Correlation of X-ray diffraction and X-ray absorption spectroscopy investigations. *Inorg. Chem.* **2015**, *54*, 11127–11135. [CrossRef]
91. Feilong, S.; Junwu, Z. Blue-green BaAl<sub>2</sub>O<sub>4</sub>: Eu<sup>2+</sup>, Dy<sup>3+</sup> phosphors synthesized via combustion synthesis method assisted by microwave irradiation. *J. Rare Earths* **2011**, *29*, 326–329.
92. Roh, H.-S.; Cho, I.-S.; An, J.-S.; Cho, C.M.; Noh, T.H.; Yim, D.K.; Kim, D.-W.; Hong, K.S. Enhanced photoluminescence property of Dy<sup>3+</sup> co-doped BaAl<sub>2</sub>O<sub>4</sub>: Eu<sup>2+</sup> green phosphors. *Ceram. Int.* **2012**, *38*, 443–447. [CrossRef]
93. Bem, D.B.; Dejene, F.; Luyt, A.; Swart, H. Luminescence studies of a combustion-synthesized blue–green BaAl<sub>x</sub>O<sub>y</sub>: Eu<sup>2+</sup>, Dy<sup>3+</sup> nanoparticles. *Phys. B Condens. Matter* **2012**, *407*, 1561–1565. [CrossRef]
94. Ryu, H.; Bartwal, K. Preparation of crystalline fibres of codoped BaAl<sub>2</sub>O<sub>4</sub>: Eu<sup>2+</sup>: Cr<sup>3+</sup>. *Cryst. Res. Technol. J. Exp. Ind. Crystallogr.* **2009**, *44*, 69–73. [CrossRef]
95. Lephoto, M.; Ntwaeeaborwa, O.; Pitale, S.S.; Swart, H.; Botha, J.; Mothudi, B.M. Synthesis and characterization of BaAl<sub>2</sub>O<sub>4</sub>: Eu<sup>2+</sup> co-doped with different rare earth ions. *Phys. B Condens. Matter* **2012**, *407*, 1603–1606. [CrossRef]
96. Kaur, J.; Jaykumar, B.; Dubey, V.; Shrivastava, R.; Suryanarayana, N. RETRACTED ARTICLE: Optical properties of rare earth-doped barium aluminate synthesized by different methods-A Review. *Res. Chem. Intermed.* **2015**, *41*, 2317–2343. [CrossRef]
97. Zhang, L.W.; Wang, L.; Zhu, Y.F. Synthesis and performance of BaAl<sub>2</sub>O<sub>4</sub> with a wide spectral range of optical absorption. *Adv. Funct. Mater.* **2007**, *17*, 3781–3790. [CrossRef]
98. Yin, X.; Lin, H.; Zhang, H.; Hong, R.; Tao, C.; Han, Z. Effect of alumina addition on the microstructure and luminescence properties of BaAl<sub>2</sub>O<sub>4</sub>: Eu<sup>2+</sup>-Al<sub>2</sub>O<sub>3</sub> green fluorescent composite ceramics fabricated by spark plasma sintering. *Ceram. Int.* **2020**, *46*, 3801–3810. [CrossRef]
99. Rodrigues, L.; Stefani, R.; Brito, H.d.; Felinto, M.; Hölsä, J.; Lastusaari, M.; Laamanen, T.; Malkamäki, M. Thermoluminescence and synchrotron radiation studies on the persistent luminescence of BaAl<sub>2</sub>O<sub>4</sub>: Eu<sup>2+</sup>, Dy<sup>3+</sup>. *J. Solid State Chem.* **2010**, *183*, 2365–2371. [CrossRef]
100. Zhang, N.-B.; Bai, C.-G.; LI, Z.-y. Preparation of BaAl<sub>2</sub>O<sub>4</sub> by microwave sintering. *Trans. Nonferrous Met. Soc. China* **2010**, *20*, 2020–2025. [CrossRef]
101. Liu, Y.L.; Tang, X.M.; Chen, X.; Lei, B.F.; Feng, D.X. Preparation of the phosphors BaAl<sub>2</sub>O<sub>4</sub>: Eu, RE (RE = Dy, Ho) by microwave heating technique and observation of long phosphorescence. *Chin. Chem. Lett.* **1999**, *10*, 709–712.
102. Huang, A.; Yang, Z.; Yu, C.; Chai, Z.; Qiu, J.; Song, Z. Tunable and white light emission of a single-phased Ba<sub>2</sub>Y(BO<sub>3</sub>)<sub>2</sub>Cl: Bi<sup>3+</sup>, Eu<sup>3+</sup> phosphor by energy transfer for ultraviolet converted white LEDs. *J. Phys. Chem. C* **2017**, *121*, 5267–5276. [CrossRef]
103. Zhang, X.; Huang, Y.; Gong, M. Dual-emitting Ce<sup>3+</sup>, Tb<sup>3+</sup> co-doped LaOBr phosphor: Luminescence, energy transfer and ratiometric temperature sensing. *Chem. Eng. J.* **2017**, *307*, 291–299. [CrossRef]
104. Wang, Q.Y.; Yuan, P.; Wang, T.W.; Yin, Z.Q.; Lu, F.C. Effect of Sr and Ca substitution of Ba on the photoluminescence properties of the Eu<sup>2+</sup> activated Ba<sub>2</sub>MgSi<sub>2</sub>O<sub>7</sub> phosphor. *Ceram. Int.* **2020**, *46*, 1374–1382. [CrossRef]
105. Dhananjaya, N.; Nagabhushana, H.; Nagabhushana, B.; Rudraswamy, B.; Shivakumara, C.; Narahari, K.; Chakradhar, R. Enhanced photoluminescence of Gd<sub>2</sub>O<sub>3</sub>: Eu<sup>3+</sup> nanophosphors with alkali (M = Li<sup>+</sup>, Na<sup>+</sup>, K<sup>+</sup>) metal ion co-doping. *Spectrochim. Acta Part A Mol. Biomol. Spectrosc.* **2012**, *86*, 8–14. [CrossRef]

- 
106. Liu, D.; Xu, X.; Du, Y.; Qin, X.; Zhang, Y.; Ma, C.; Wen, S.; Ren, W.; Goldys, E.M.; Piper, J.A. Three-dimensional controlled growth of monodisperse sub-50 nm heterogeneous nanocrystals. *Nat. Commun.* **2016**, *7*, 1–8. [[CrossRef](#)] [[PubMed](#)]
  107. Sui, Y.; Tao, K.; Tian, Q.; Sun, K. Interaction between  $Y^{3+}$  and oleate ions for the cubic-to-hexagonal phase transformation of  $NaYF_4$  nanocrystals. *J. Phys. Chem. C* **2012**, *116*, 1732–1739. [[CrossRef](#)]